Renewable Energy 181 (2022) 692–713

Contents lists available at ScienceDirect

Renewable Energy

journal homepage: www.elsevier.com/locate/renene

A semi-coupled aero-servo-hydro numerical model for floating vertical axis wind turbines operating on TLPs

Ju Gao [a], D. Todd Griffith [a, *], Mohammad Sadman Sakib [a], Sung Youn Boo [b]

[a] Department of Mechanical Engineering, University of Texas at Dallas, Richardson, TX, 75080, USA
[b] VL Offshore, Houston, TX, 77084, USA

ARTICLE INFO

Article history:
Received 8 April 2021
Received in revised form
16 September 2021
Accepted 18 September 2021
Available online 21 September 2021

Keywords:
Floating vertical axis wind turbine
7-DOF model
Tension leg platform
Structural dynamics
Hydrodynamics

ABSTRACT

Floating vertical axis wind turbines (VAWTs) have many advantages over floating horizontal axis wind turbines (HAWTs) at large scales in deep water; however, there are several key challenges to overcome as well. One of the challenges is accurate prediction of the dynamic motion and loads performance of a floating VAWT. A new semi-coupled aero-servo-hydro method is developed to assess dynamic responses of a floating VAWT by modeling the system as a 7-degree-of-freedom (7-DOF) model: the supporting platform is considered as a 6-DOF rigid body; the rotation of the rotor is considered as the 7th DOF. Aerodynamic, hydrodynamic, and mooring loads and control of the rotor speed are fully considered. This model can predict performance of floating VAWTs with reasonable fidelity according to validation with OrcaFlex through static and dynamic responses of a floating VAWT with Darrieus rotor operating on a new tension-leg platform (TLP). Being a reduced complexity model, the 7-DOF model can be efficiently applied to assess performance of the newly designed floating VAWT. This model is used to examine the relative contributions of aerodynamic and wave loads imparted to the floating system and the benefits of a three-bladed VAWT over a two-bladed VAWT through dynamic and fatigue analysis.

1. Introduction

Development of floating offshore wind turbines (FOWTs) in very deep waters for greater wind resources is booming. Floating vertical axis wind turbines (VAWTs) are back to the interest of researchers due to their advantages over floating horizontal axis wind turbines (HAWTs). Floating HAWTs at large scales have limitations and disadvantages such as the fatigue issue of turbine blades caused by cyclic gravity loads, high position of transmission and generation system requiring stronger tower, difficulty of installation, in contrast, floating VAWTs at large scales have advantages such as decreased fatigue damage of blades due to smaller rotor speeds and no cyclic gravity loads on blades, and low machinery position easier to install and maintain [1,2]. There is one more important advantage of floating VAWTs over floating HAWTs that the supporting platform of a VAWT is smaller in size, needs less steel mass, and more cost-effective comparing with that of a HAWT [3].

The nonlinear coupling effect between aerodynamics and hydrodynamics brings challenge to study dynamic responses of floating wind turbines. A number of fully coupled aero-hydro-servo-elastic time-domain dynamic simulation tools for floating HAWTs have been developed and well validated. The FAST (Fatigue, Aerodynamics, Structures, and Turbulence) [4] is a well-known open source tool developed by the National Renewable Energy Laboratory (NREL), which is coupled with an aerodynamics module and a hydrodynamics module to consider aerodynamic and hydrodynamic loads. FAST is one of the most popularly used tools for initial design of HAWTs. OpenFAST [5] is a more sophisticated open source tool built on FAST by NREL. FAST is also commonly used to couple with in-house codes developed by different institutes for better hydrodynamic performance. The CHARM3D program [6] is developed to implement FAST into the floater-mooring coupled dynamic analysis model. A fully coupled framework (F2A) [7] is developed based on FAST and AQWA (an advanced commercial hydrodynamic analysis program) [8] by utilizing AQWA to enhance hydrodynamic simulation capabilities for FOWTs. The industrial software Bladed [9,10] is an integrated tool providing dynamic simulation and optimization of wind turbines. It utilizes multibody dynamic approach to formulate the structural dynamics of wind

* Corresponding author.
E-mail addresses: ju.gao@utdallas.edu (J. Gao), tgriffith@utdallas.edu (D.T. Griffith), Sadman.Sakib@utdallas.edu (M.S. Sakib), sboo@vloffshore.com (S.Y. Boo).

https://doi.org/10.1016/j.renene.2021.09.076
0960-1481/

turbines. It is able to model both fixed and floating platforms by building platforms in its interface or imported from offshore design tools. Advanced hydrodynamic properties can also be considered by importing from the commercial software WAMIT [11], AQWA, and so on. A fully coupled multibody method based on sequenced Euler angles, the momentum cloud method, is developed for FOWTs without restriction of small angle assumption [12,13]. The program, Dynamic Analysis for Response of Wind Turbines (DARwind) [14], simulates motions of FOWTs based on Kane's dynamic method and calculates hydrodynamic loads based on hydrodynamic coefficients output from WAMIT. The combined SIMO/RE-FLEX/AeroDyn tool [15] can also be used to simulate the coupled FOWT system.

The industrial aeroelastic code HAWC2 (short for Horizontal Axis Wind turbine simulation Code 2nd generation) [16] solves wind turbine response in time domain based on multibody formulation and can consider wave loads based on Morison's equation or using hydrodynamic coefficients output from software such as WAMIT. DeepLines [17,18] is a fully coupled software developed based on the finite element method. It simulates blades, tower, drivetrain, and moorings with nonlinear beam elements, calculates hydrodynamic loads using hydrodynamic coefficients, and considers aerodynamic loads by external aerodynamic libraries. The finite element method is commonly used to solve wind turbine dynamics [17,19]. These two tools can be used to simulate both floating HAWTs and floating VWATs.

The studies of floating VAWTs are not as much as those of floating HAWTs. Increasing sizes of floating VAWTs require larger floating platforms to deal with the larger aerodynamic and gravity loads. The calculation of aerodynamic loads of VAWTs is more complex than that of HAWTs. CACTUS (short for Code for Axial and Cross-flow TUrbine Simulation) [20] is developed to simulate the aerodynamic performance of both HAWTs and VAWTs based on a free wake vortex method. A two-dimensional actuator cylinder flow model is adapted to calculate the three-dimensional aeroelastic loads of VAWTs in HAWC2 code in time domain [21]. The software QBlade [22,23] can also be used for the simulation and design of both HAWTs and VAWTs. It applies the Blade Element Momentum (BEM) method to HAWTs and Double Multiple Streamtube (DMS) algorithm as well as the nonlinear Lifting Line Theory (LLT) to VAWTs' simulations.

There are some tools applied to study floating VAWTs. The Offshore Wind ENergy Simulation (OWENS) toolkit [24] is a design tool solving the dynamic responses of VAWTs based on the finite element method. The modal analysis results computed using OWENS have been validated with experimental data of a 34 *m* VAWT test bed. Reaction loads at tower base output from OWENS can be transferred as the input loads to platform, then the platform dynamic responses can be assessed based on the uncoupled loads. An aero-hydro-servo-elastic coupled model of dynamics for floating VAWTs called FloVAWT (short for Floating Vertical Axis Wind Turbine) [25–27] is designed and further validated with experimental data. This fully coupled model calculates aerodynamic loads based on the DMS model; it also considers the floating structure as a rigid body and computes hydrodynamic loads using hydrodynamic coefficients; its mooring module is simulated based on quasi-static catenary equations. The Simo-Riflex-DMS simulation tool [28] simulates a floating VAWT as an integrated dynamic model including the aerodynamics, hydrodynamics, structural dynamics, and generator control. It assumes the floating structure as a rigid body and computes its motion based on the linear hydrodynamic theory including viscous drag loads from Morison's equation; it models the turbine and moorings as flexible elements based on the non-linear finite element code; and it calculates aerodynamic loads using the DMS model. Later, Cheng et al. [29] apply this Simo-Riflex-DMS code to study dynamic responses of floating VAWTs with a two-bladed Darrieus rotor and three types of floating platforms, which are spar, semi-submersible, and TLP, respectively. Pitance et al. [30] develop an aero-servo-elastic code called PHARWEN3D for VAWTs, which couples a free wake vortex code ARDEMA3D (short for Areva-Delft-Madrillet) [31], a structural simulation code developed based on beam-element theory, and a wind turbine controller code. This code can be applied as input to rigid-body motions such as a floating VAWT. Another fully coupled tool Simo-Riflex-AC [32] including the aerodynamics, hydrodynamics, structural dynamics and controller dynamics is developed based on the actuator cylinder flow model and compared with the HAWC2 code and Simo-Riflex-DMS tool. A new servo-hydro simulation code [33] is developed to study FOWTs by coupling the dynamic multibody software InWave [34] with CACTUS. It can be applied for both HAWTs and VAWTs. The commonly used commercial software OrcaFlex [35] for mooring analysis of offshore oil and gas platforms is extended for floating renewable energy foundations. It solves nonlinear dynamic mooring coupled with floating foundation in time domain. The mooring lines are modeled using a finite element method considering buoyancy, weight, viscous drag, hydrodynamic loads and so on, thus the results from OrcaFlex are more accurate than the results from a quasi-static model. OrcaFlex is a semi-coupled analysis tool since it considers time series of aerodynamic loads as external loads so that the platform is coupled with the turbine while the turbine is decoupled to the platform.

Several floating VAWT concepts and designs have been proposed in recent years. Vita et al. [36] propose a new floating VAWT concept with a two- or three-bladed Darrieus rotor and a submerged buoy-like floater for deep water and large turbines. They design a 2 MW rotor with rotor radius equal to 40 m and a 20 MW one with 120 m radius. Later, Paulsen et al. [37,38] present their first 5 MW baseline design for the DeepWind concept including a two-bladed Darrieus VAWT and a spar type floater for water depths more than 150 m. Akimoto et al. [39] propose a new concept that a floating VAWT has a tilted axis to balance the turbine thrust, buoyancy and gravity. Their initial study shows the feasibility to reduce the system weight by allowing large tilt angles. Sutherland et al. [40] have designed a Sandia 34-m VAWT test bed, a full-Darrieus VAWT, for further research in aerodynamics, structural dynamics, fatigue life prediction, and control algorithms. Collu et al. [27] design two floating platforms supporting VAWTs including a barge and a semi-submersible in order to study the feasibility of a floating VAWT with power generation between 10 and 20 MW. They conclude that the basic design requirements for floaters to support VAWTs such as the abilities to float and counteract the wind turbine overturning moment are not enough, and the driving requirement is their reasonable dynamic responses to wave loads. Griffith et al. [3] compare aerodynamic performance of both Darrieus and V-VAWT type VAWTs and study hydrodynamic performance of spar and semi-submersible type floating platforms supporting VAWTs as well as the costs of both platforms. Griffith et al. [2] develop innovative VAWT rotor designs for offshore wind turbines and assess the dynamic performance of floating platforms supporting large scale 5 MW VAWTs. Savenije [41] presents the design of a semi-submersible tri-floater to support a 6 MW two-bladed H-Rotor type VAWT for the Semi-Submersible Support Structure for Vertical Axis Wind Turbine (S4VAWT) project. This study concludes that the designed floater is 20% lighter than the platform for a HAWT with the same rated power, which is in-line with findings also in Ref. [3].

The present study develops an aero-servo-hydro coupled model for dynamic simulations of floating VAWTs in both time and frequency domains. The newly developed model represents a floating

VAWT as a 7-DOF model, in which the floating platform is considered as a rigid body with 6 DOFs and the rotation of the rotor is taken as the 7th DOF. The input aerodynamic loads acting on the VAWT and the torque load for the 7th DOF can be computed using CACTUS, the hydrodynamic loads acting on the platform can be calculated using hydrodynamic coefficients output from the commercial software WAMIT or the open source code Capytaine [42], and the mooring loads can be computed using the open source code MoorDyn [43] developed based on the lumped-mass method. This semi-coupled model can solve dynamic responses of a floating structure combining with the effect from its rotating top structure considering the above-mentioned loads. Validation of this simplified 7-DOF model is accomplished with the commercial dynamic analysis software OrcaFlex.

This 7-DOF model can be easily applied to study motions of floating VAWTs without considering the complexity of transformations among multi-bodies. The simulation tool developed based on the 7-DOF model has the potential to reduce computation time comparing with other fully coupled simulation tools since both aerodynamic and hydrodynamic loads are pre-calculated and not required to compute at each time step based on the instantaneous positions of the structures. Moreover, the matrix size in the solution is largely decreased due to the less DOFs in this model. Strength and fatigue analyses of moorings can be assessed based on mooring tensions output from the simulation tool. Thus this new model can be easily applied to initially design and optimize floating VAWT systems. One more advantage of this model is that the rotor speed control strategy can be easily implemented to the 7th DOF.

Two newly designed floating VAWTs are introduced in this study. A series of performance comparison between the two-bladed and three-bladed floating VAWTs is evaluated using the 7-DOF model including platform motions and tendon tensions under different environmental conditions, power performance, and fatigue performance of tendons. The advantages and disadvantages of a two-bladed floating VAWT over a three-bladed floating VAWT are obtained based on these comparative results. In addition, the impacts from various individual load components on the performance of platform motions and tendon tensions are evaluated to provide guidance for future control study and design of the mooring tendons.

The UTD 5 MW baseline VAWTs with the supported TLPs used in this study are described in Section 2; the 7-DOF model and its solution methodologies as well as validation of the developed simulation tool with OrcaFlex are presented in Section 3; design studies using the 7-DOF model including effects of different load components on floating VAWTs, comparative dynamic responses between two- and three-bladed VAWTs, and platform responses under intra-cycle angular velocity control (also called intra-cycle RPM control for simplicity, and RPM represents angular velocity in revolution per minute) on the 7th DOF are presented in Section 4; and conclusions are presented in Section 5.

2. Floating VAWT models

A floating VAWT is composed of one rotor and one supporting floater. The rotor sitting on top of the floater rotates around its own axis under operating condition. Station keeping of the floater is provided by moorings. Two newly designed 5 MW Darrieus rotors [44] are used in this study shown in Fig. 1: one with two blades and the other with three blades. The rotor consists of two or three blades and one tower. Blades are fixed to the tower at both ends and strength of each blade is enhanced through two struts which connect between blade and tower. The generator is assumed to be installed at the tower base. Both rotors have same solidity and rated power. Detailed characteristics of the two rotors are presented in Table 1.

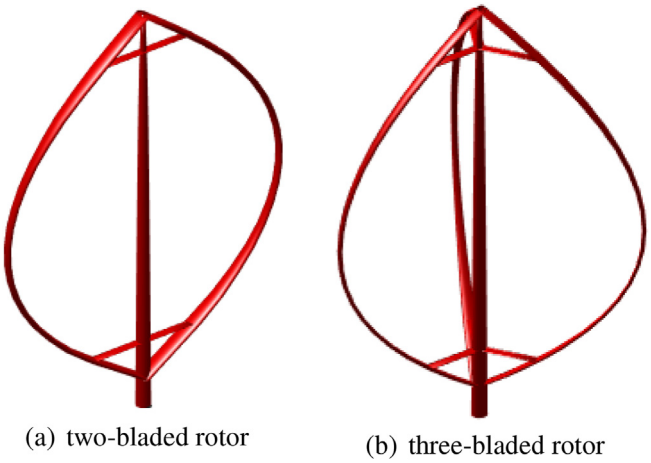

Fig. 1. Two-bladed and three-bladed Darrieus rotors.

Two initially designed TLP-type floaters which were developed from the TLP wind designs [45,46] are applied as the supporting floaters for the two- and three-bladed rotors in deep water, respectively. The TLPs contain one center column where the tower is located and three outer columns connecting with the center column by three rectangular pontoons, respectively. Each outer column is connected with one mooring tendon which is always in tension. The motions of the TLPs especially the heave, roll, and pitch motions are limited by the tendons. Table 2 summarizes main properties of the two floating VAWTs. CoG in the table represents the center of gravity of the floating VAWT. Fig. 2 shows the configuration of the two-bladed floating VAWT used in this study. CoP in the figure represents the aerodynamic pressure center of the rotor, where wind loads are applied. The tendon layout is also illustrated with T1, T2, and T3 representing the three tendons, respectively.

The flutter analysis of the two- and three-bladed VAWTs is done in another study [47]. The hard tower flutter mode is found to be a potential concern at the lowest rotor speed. Both modal and flutter characteristics of the newly designed two floating VAWTs are also assessed and Campbell diagrams are generated to evaluate the resonant issues during operating conditions. No resonant issue is found at the operating rotor speed, but there is a concern at low rotor speed such as the start-up or shutdown of the turbine due to the per-rev crossings of the lowest frequency rigid body modes.

3. A newly developed 7-DOF model for floating VAWTs

3.1. Development of a 7-DOF model in time domain

The floating VAWT is considered as a rigid body plus the rotating rotor in the 7-DOF model. The rigid body has six degrees of freedom and the rotor has one rotating degree, which is represented as the 7th degree of the system. Two coordinate systems (CS) are applied to the 7-DOF model including the global fixed CS (X-Y-Z) and the body-fixed CS (x-y-z). Fig. 2 shows the global CS of the two-bladed floating VAWT. The origin of the global CS is located at the center of gravity of the whole structure, the positive X-axis is along the direction with the wave angle heading of zero, the positive Z-axis is pointed upwards, and the positive Y-axis is defined by the right-hand rule; the body-fixed CS coincides with the global CS when the system is undisplaced. The translational and rotational displacements of the structure of the first six DOFs can be expressed as a vector:

Table 1
Specifications of two 5 MW Darrieus rotors.

	Unit	5 MW 2B VAWT	5 MW 3B VAWT
Number of blades	–	2	3
Rated power	MW	5	5
Rotor equatorial radius	m	54.1	54.1
Blade length	m	177.1	177.8
Tower height	m	142.1	142.1
Rotor mass (blades + struts + tower)	kg	220,480	322,252
Generator mass	kg	434,000	434,000
CoG of rotor and generator above tower base	m	21.1	28.8
Rated rotor speed	rpm	7.8	7.9
Cut-in wind speed	m/s	5	5
Rated wind speed	m/s	15	15
Cut-out wind speed	m/s	25	25

Table 2
Characteristics of two TLP-type floating VAWTs.

	Unit	Floating VAWT (2B)	Floating VAWT (3B)
Water depth	m	100	100
Draft	m	15	15
Total mass (turbine + hull + ballast)	ton	1981	2148
Buoyancy in undisplaced position	ton	3302	3465
CoG above MWL	m	6.7	10.0
Radius of gyration about CoG: Roll	m	30.3	36.9
Radius of gyration about CoG: Pitch	m	30.3	36.9
Radius of gyration about CoG: Yaw	m	16.4	19.6

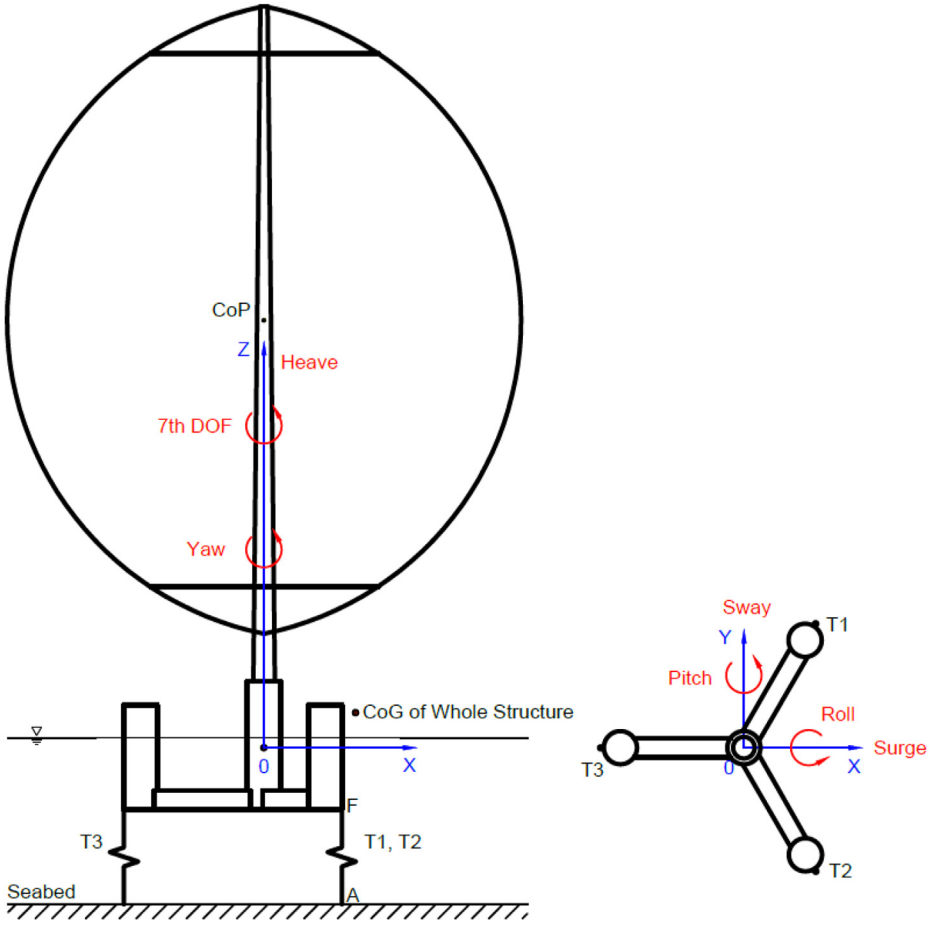

Fig. 2. Floating VAWT configuration and coordinate system of a 7-DOF two-bladed system.

$$\vec{X} = [X_1 \quad X_2 \quad X_3 \quad X_4 \quad X_5 \quad X_6]^T \tag{1}$$

where X_1, X_2, and X_3 represent surge, sway, and heave motions, X_4, X_5, and X_6 indicate rotations in the roll, pitch, and yaw directions. The transformation matrix between the global CS and the body-fixed CS conforming to the roll-pitch-yaw Euler angle sequence is expressed as:

$$T_{B\to G} = \begin{bmatrix} cX_5cX_6 & -cX_5sX_6 & sX_5 \\ cX_4sX_6 + sX_4sX_5cX_6 & cX_4cX_6 - sX_4sX_5sX_6 & -sX_4cX_5 \\ sX_4sX_6 - cX_4sX_5cX_6 & sX_4cX_6 + cX_4sX_5sX_6 & cX_4cX_5 \end{bmatrix} \tag{2}$$

where cX_i represents $\cos(X_i)$ and sX_i represents $\sin(X_i)$, the subscript i indicates the DOF.

The floating VAWT is usually assumed as one rigid body with six DOFs in some other simulation tools. The dynamic responses of the whole structure are solved using the following equation of motion:

$$[M + A(\infty)]\ddot{X}(t) + \int_0^t K(t-\tau)\dot{X}(\tau)d\tau + (C_h + C_m)X(t) = F_{ext}(t) \tag{3}$$

where M is the mass matrix of the whole structure, $A(\infty)$ is the added mass at infinite frequency of the structure, C_h and C_m are hydrostatic and mooring restoring stiffness matrices, respectively, $F_{ext}(t)$ represents the external loads acting on the structure including wind, wave, and current loads ($F_{ext} = F_{wind} + F_{wave} + F_{current}$). $K(t)$ is the impulse response function:

$$K(t) = \frac{2}{\pi}\int_0^\infty B(\omega)cos(\omega t)d\omega \tag{4}$$

where $B(\omega)$ represents the damping coefficient in frequency domain. The convolution term in Equation (3) represents the memory effect from the water and can be computed using numerical integral method such as trapezoidal rule or Simpson rule.

Equations of motion (EOMs) of the 7-DOF system in time domain are set up in the global CS based on the 6-DOF EOMs and can be expressed in matrix form as:

$$\begin{bmatrix} M_{6\times6} + A_{6\times6}(\infty) & 0_{6\times1} \\ 0_{1\times6} & I_{wt} \end{bmatrix} \begin{bmatrix} \ddot{X}_{6\times1}(t) \\ \ddot{X}_7(t) \end{bmatrix} + \begin{bmatrix} K_{t6\times6}(t) & 0_{6\times1} \\ 0_{1\times6} & B_{wt} \end{bmatrix} \begin{bmatrix} \dot{X}_{6\times1}(t) \\ \dot{X}_7(t) \end{bmatrix} + \begin{bmatrix} C_{6\times6} & 0_{6\times1} \\ 0_{1\times6} & C_{wt} \end{bmatrix} \begin{bmatrix} X_{6\times1}(t) \\ X_7(t) \end{bmatrix} = \begin{bmatrix} F_{6\times1}(t) \\ T_7(t) \end{bmatrix} \tag{5}$$

where $X_{6\times1}(t)$, $\dot{X}_{6\times1}(t)$, and $\ddot{X}_{6\times1}(t)$ represent displacement, velocity, and acceleration vector of the first six DOFs of the system with respect to surge, sway, heave, roll, pitch, and yaw motions, respectively, $X_7(t)$ represents the rotational motion of the rotor around the Z-axis, which is the azimuth angle of the rotor, $M_{6\times6}$ is the mass matrix of the system (including the platform and the rotor) except the inertia of the rotor around the Z-axis, $A_{6\times6}(\infty)$ is the added mass at infinite frequency of the system, I_{wt} is the inertia of the rotor about the Z-axis, $K_{t6\times6}(t)$ represents the part of radiation loads calculated from the impulse response function related to current time step, B_{wt} is the damping of the rotor, $C_{6\times6}$ represents the hydrostatic restoring stiffness and/or restoring mooring stiffness matrix of the system, C_{wt} is the stiffness of the rotor, $F_{6\times1}(t)$ represents hydrodynamic load acting on the platform plus thrust, lateral force, and generator torque acting on the rotor, mooring load may be also included depending on which method is used to calculate the mooring load, $T_7(t)$ is the difference between aerodynamic torque and generator torque of the rotor. The equation of motion of the 7th DOF can be presented as:

$$I_{wt}\ddot{X}_7 + B_{wt}\dot{X}_7 + C_{wt}X_7 = T_7 = T_{aero} - T_{generator} \tag{6}$$

where $X_7 = \theta$ represents the rotational angle of the rotor, $\dot{X}_7 = \dot{\theta} = \omega$ represents the angular velocity of the rotor, and $\ddot{X}_7 = \ddot{\theta} = \dot{\omega}$ is the angular acceleration of the rotor.

3.1.1. Hydrodynamics

The hydrodynamic loads can be computed using the potential flow theory combining with the Morison's equation. The added mass coefficients, damping coefficients, and wave excitation forces in Equations (3)–(5) can be calculated using the potential flow theory and obtained from the industrial software WAMIT or the open source code Capytaine. The viscous drag loads acting on the platform can be implemented using the Morison's equation with only the quadratic drag term considered as below:

$$F_{drag} = \frac{1}{2}\rho C_D D(u-v)|u-v| \tag{7}$$

where ρ is the water density, C_D is the drag coefficient, D is the diameter of the cylindrical column, u and v are the water particle velocity and the platform velocity, respectively, $u - v$ is the relative velocity between water and structure.

The viscous loads can also be added through linear damping force alternatively as below:

$$F_{viscous} = -C_v\dot{X} \tag{8}$$

where C_v represents the linear viscous damping coefficient.

3.1.2. Mooring dynamics

The tension at the top of one mooring tendon can be computed using the instantaneous positions at the fairlead to account for effects of the translational and rotational platform motions. Vectors $[X_{1F} \quad X_{2F} \quad X_{3F}]^T$ and $[X_{1A} \quad X_{2A} \quad X_{3A}]^T$ representing the fairlead and anchor instantaneous positions of tendon 1 (T1 in the tendon layout shown in Fig. 2) in the global CS can be expressed as:

$$\begin{bmatrix} X_{1F} \\ X_{2F} \\ X_{3F} \end{bmatrix} = \begin{bmatrix} X_1 \\ X_2 \\ X_3 \end{bmatrix} + T_{B\to G}\begin{bmatrix} L_{OF} \times \cos\frac{\pi}{3} \\ L_{OF} \times \sin\frac{\pi}{3} - Draft \end{bmatrix} \tag{9}$$

$$\begin{bmatrix} X_{1A} \\ X_{2A} \\ X_{3A} \end{bmatrix} = \begin{bmatrix} L_{OF} \times \cos\frac{\pi}{3} \\ L_{OF} \times \sin\frac{\pi}{3} - WDpth \end{bmatrix} \tag{10}$$

where L_{OF} is the distance from the origin of the body-fixed CS to the fairlead of T1, $Draft$ is the draft of the platform, $WDpth$ is the water depth. Tension vector $\vec{F}_{T1}$ and moment vector $\vec{M}_{T1}$ of T1 are then computed as below [48]:

$$\vec{F}_{T1} = \left[T_0 + \frac{ES}{L}\left(\left|\vec{F}\,\vec{A}\right| - L\right)\right]\frac{\vec{F}\,\vec{A}}{\left|\vec{F}\,\vec{A}\right|} \tag{11}$$

$$\vec{M}_{T1} = r_{OF} \times \vec{F}_{T1} \tag{12}$$

where $\vec{F}\,\vec{A}$ is the distance vector from the fairlead to the anchor which can be computed using the position vectors $[X_{1F} \quad X_{2F} \quad X_{3F}]^T$ and $[X_{1A} \quad X_{2A} \quad X_{3A}]^T$, $\left|\vec{F}\,\vec{A}\right|$ is the length of $\vec{F}\,\vec{A}$, r_{OF} is the distance vector from the fairlead to the origin of the global CS. This method takes into account the instantaneous locations of the tendons; however, it only calculates tensions by neglecting the tendon weight, buoyancy, and wave effects acting on the tendons.

A lumped-mass mooring line model has been developed to solve mooring tensions taking into account weight, buoyancy, axial stiffness and damping forces, hydrodynamic forces from Morison's equation, and vertical spring-damper forces from contact with the seabed except wave kinematics [43]. Moorings in this model are divided into segments of equal length, which are connected with nodes. The equation of motion for each node on one mooring is set up and solved using the Runge-Kutta integration algorithm. In this study, MoorDyn, an open source mooring line model developed based on this lumped-mass model is introduced to model the mooring tendon and coupled with the present 7-DOF model. Tensions at tendon tops calculated using MoorDyn are passed to the 7-DOF model as the tendon loads acting on the platform.

These two methods to calculate tendon loads are compared in terms of offset vs. set-down shown in Section 3.3.1.

3.1.3. Aerodynamics

Aerodynamic loads on the floating VAWTs are computed using a free wake vortex method. Steady and uniform inflows are considered in this study [44]. Fig. 3 shows comparisons of aerodynamic load components including thrust, lateral force, and torque for one revolution at the rated (15 m/s) wind speed in the 0° direction between two-bladed and three-bladed turbines. Thrust is along the wind direction (namely positive X-axis) and lateral force is perpendicular to thrust (along positive Y-axis). Aerodynamic loads of the two-bladed turbine are observed to have two periods in one rotor revolution and those of the three-bladed turbine have three periods due to the symmetry of the turbines. The strong twice-per-revolution (2P) and three-per-revolution (3P) effects from aerodynamic loads may introduce great impacts on mooring fatigue life, especially for tendons of TLPs. Detailed fatigue assessments are illustrated in Section 4 to further study these periodic effects. Amplitudes of thrust, lateral force, and torque of the three-bladed turbine are only 20%, 21%, and 27% of the two-bladed turbine, respectively. Mean values of load components are almost same for both turbines as illustrated in Table 3. The thrust and lateral force mainly result in offset of the supporting platform. It can be estimated that thrust with a positive mean value leads to a positive mean platform motion in the same direction as thrust, while lateral force with a zero mean results in a zero-mean motion in the lateral force direction. This implies that better structural dynamic performance of the three-bladed floating VAWT is expected due to smaller aerodynamic loads comparing with the two-bladed floating VAWT.

3.2. Development of a 7-DOF model in frequency domain

Simulation in frequency domain requires much shorter computing time than that in time domain, but non-linear effects are omitted in frequency domain solution. Equations of motion of a 6-DOF rigid floating VAWT in frequency domain can be expressed as:

Table 3
Statistics of aerodynamic load components at 15 m/s wind speed.

Aerodynamic Load	Thrust [kN]		Lateral Force [kN]		Torque [kN-m]	
Number of Blades	2	3	2	3	2	3
Maximum	921	567	609	116	11435	8091
Minimum	28	386	−567	−127	−40	4950
Mean	488	480	−2	0	6106	6408

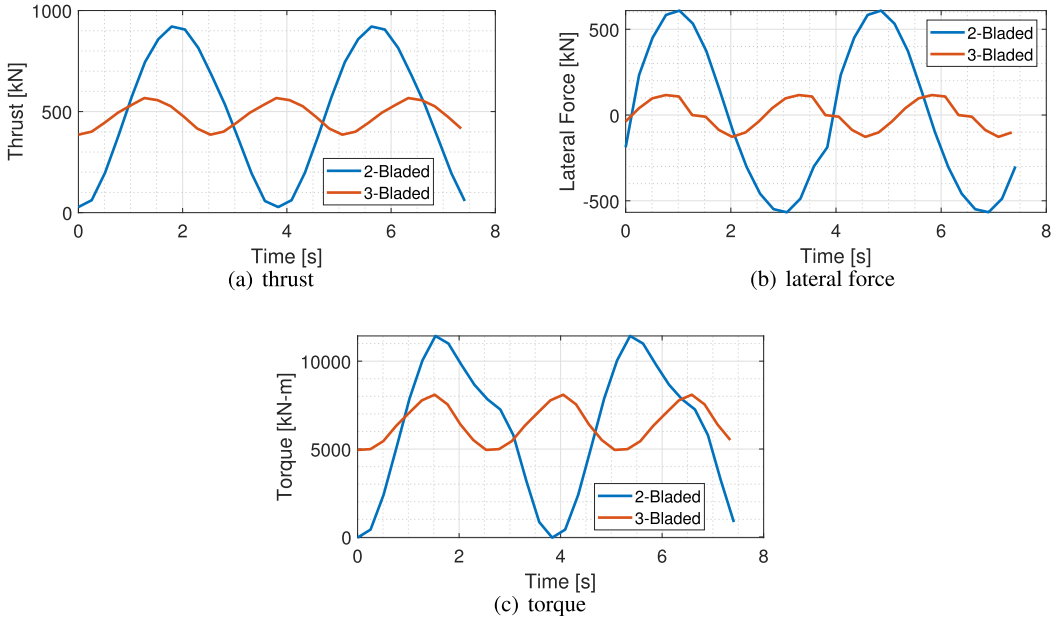

Fig. 3. Aerodynamic load components of 2- and 3-bladed turbines at 15 m/s wind speed.

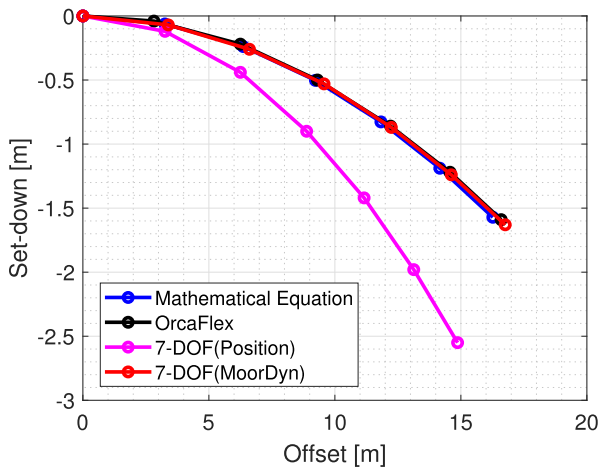

Fig. 4. Comparison of offset vs. set-down among theoretical equation, OrcaFlex, and the 7-DOF model.

Table 4
Natural periods and frequencies of the two-bladed floating VAWT.

	Natural Period		Natural Frequency		Difference
	[s]		[rad/s]		[%]
DOF	OrcaFlex	7-DOF	OrcaFlex	7-DOF	
Surge	36.12	38.25	0.17	0.16	5.88
Sway	36.12	38.25	0.17	0.16	5.88
Heave	1.78	1.72	3.53	3.65	3.40
Roll	1.82	1.78	3.45	3.53	2.32
Pitch	1.80	1.76	3.49	3.57	2.29
Yaw	24.68	26.22	0.25	0.24	4.00

$$\left[-\omega^2(M+A(\omega))+i\omega B(\omega)+(C_h+C_m)\right]X(\omega)=F(\omega) \tag{13}$$

where $A(\omega)$ and $B(\omega)$ are the hydrodynamic frequency-dependent added mass matrix and damping matrix, respectively, $X(\omega)$ is displacement complex vector, $F(\omega)$ is the frequency-dependent excitation force from wind and wave.

Equations of motion of the 7-DOF model in frequency domain can be expressed based on the 6-DOF EOMs as:

$$\begin{bmatrix} M_{6\times6}+A_{6\times6}(\omega) & 0_{6\times1} \\ 0_{1\times6} & I_{wt} \end{bmatrix}\begin{bmatrix} \ddot{X}_{6\times1}(\omega)\ddot{X}_7(\omega) \end{bmatrix}+\begin{bmatrix} B_{6\times6}(\omega) & 0_{6\times1} \\ 0_{1\times6} & B_{wt}(\omega) \end{bmatrix}$$
$$\begin{bmatrix} \dot{X}_{6\times1}(\omega) \\ \dot{X}_7(\omega) \end{bmatrix}+\begin{bmatrix} C_{6\times6} & 0_{6\times1} \\ 0_{1\times6} & C_{wt} \end{bmatrix}\begin{bmatrix} X_{6\times1}(\omega) \\ X_7(\omega) \end{bmatrix}=\begin{bmatrix} F_{6\times1}(\omega) \\ T_7(\omega) \end{bmatrix} \tag{14}$$

where $\ddot{X}_{6\times1}(\omega)$ and $\dot{X}_{6\times1}(\omega)$ represent acceleration and velocity complex vectors of the floating VAWT, $B_{wt}(\omega)$ is the damping coefficient of the VAWT around the Z-axis, $T_7(\omega)$ is the difference between aerodynamic torque and generator torque of the VAWT in frequency domain.

3.3. Validation of the 7-DOF model for floating VAWTs

Both static and dynamic tests of the two-bladed floating VAWT are carried out to validate the 7-DOF model against OrcaFlex. Validation process starts with offset vs. set-down comparison which can show a TLP system stiffness; then free decay tests are followed to determine the natural frequencies of the floating VAWT. Dynamic responses of the floating VAWT for two simulation cases, one with only turbine aerodynamic loads and the other one with both aerodynamic and regular wave loads, are additionally compared with the results from OrcaFlex.

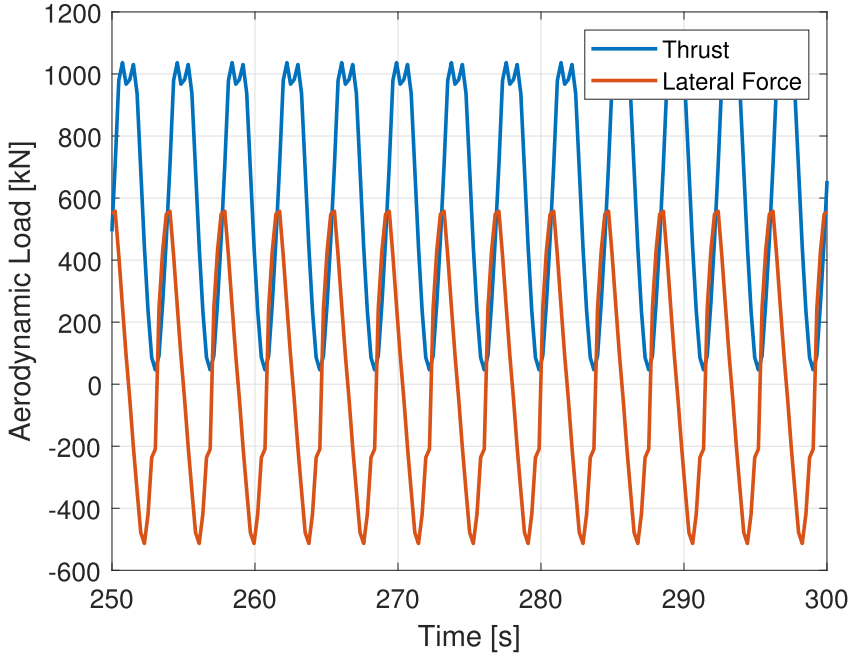

Fig. 5. Time series of aerodynamic loads used in the validation.

The analysis procedure of the semi-coupled 7-DOF model is similar to that of OrcaFlex. For both tools, in the time domain, decoupled aerodynamic loads applied to the floating system are pre-calculated using a free wake vortex method in CACTUS, interpolated and then applied to the rotor pressure center at each time step. Coupled wave loads are computed using hydrodynamic coefficients output from a diffraction analysis software such as WAMIT. However, coupled nonlinear restoring loads from moorings are achieved from different mooring models in these two tools. At each time step in the 7-DOF model, platform motions are taken as the inputs to MoorDyn and then mooring reaction loads are internally computed based on the lumped-mass method and then output from MoorDyn to the system. In OrcaFlex, a full finite element solution is used to compute mooring loads.

3.3.1. Offset vs. set-down

The TLP has limited motion in the vertical direction because of its high axial stiffness. Its lateral offset (excursion) results in a vertical displacement called set-down. The relationship between offset and set-down can be calculated using mathematical equations [49]:

$$F_H = \left(2X_{3N} - X_{3N}^2\right)^{1/2}(T_{0N} + X_{3N})(1 - X_{3N})^{-1} \tag{15}$$

$$F_H = X_{1N}\left(1 - X_{1N}^2\right)^{-1/2}(1 + T_{0N}) - X_{1N} \tag{16}$$

where F_H, T_{0N}, X_{1N}, and X_{3N} are non-dimensional forms of horizontal force, pre-tension, offset, and set-down, respectively. These terms are derived by the variables including tendon length L, water density ρ, gravitational acceleration g, area of water plane A_{wp} and expressed as $F_H = F_h/\rho g A_{wp} L$, $T_{0N} = T_0/\rho g A_{wp} L$, $X_{1N} = X_1/L$, and $X_{3N} = X_3/L$, where F_h, T_0, X_1, and X_3 are dimensional forms of horizontal force, pre-tension, offset, and set-down, respectively.

Fig. 4 shows the comparison of offset vs. set-down among the mathematical equation method, OcaFlex, and two mooring methods in the 7-DOF model. As described in Section 3.1.2, the instantaneous positions of moorings and the lumped-mass method are applied to compute mooring loads in the 7-DOF model. 7-DOF(Position) and 7-DOF(MoorDyn) in the figure represent these two methods, respectively. The curves computed using the mathematical equation, OcaFlex, and 7-DOF(MoorDyn) match very well.

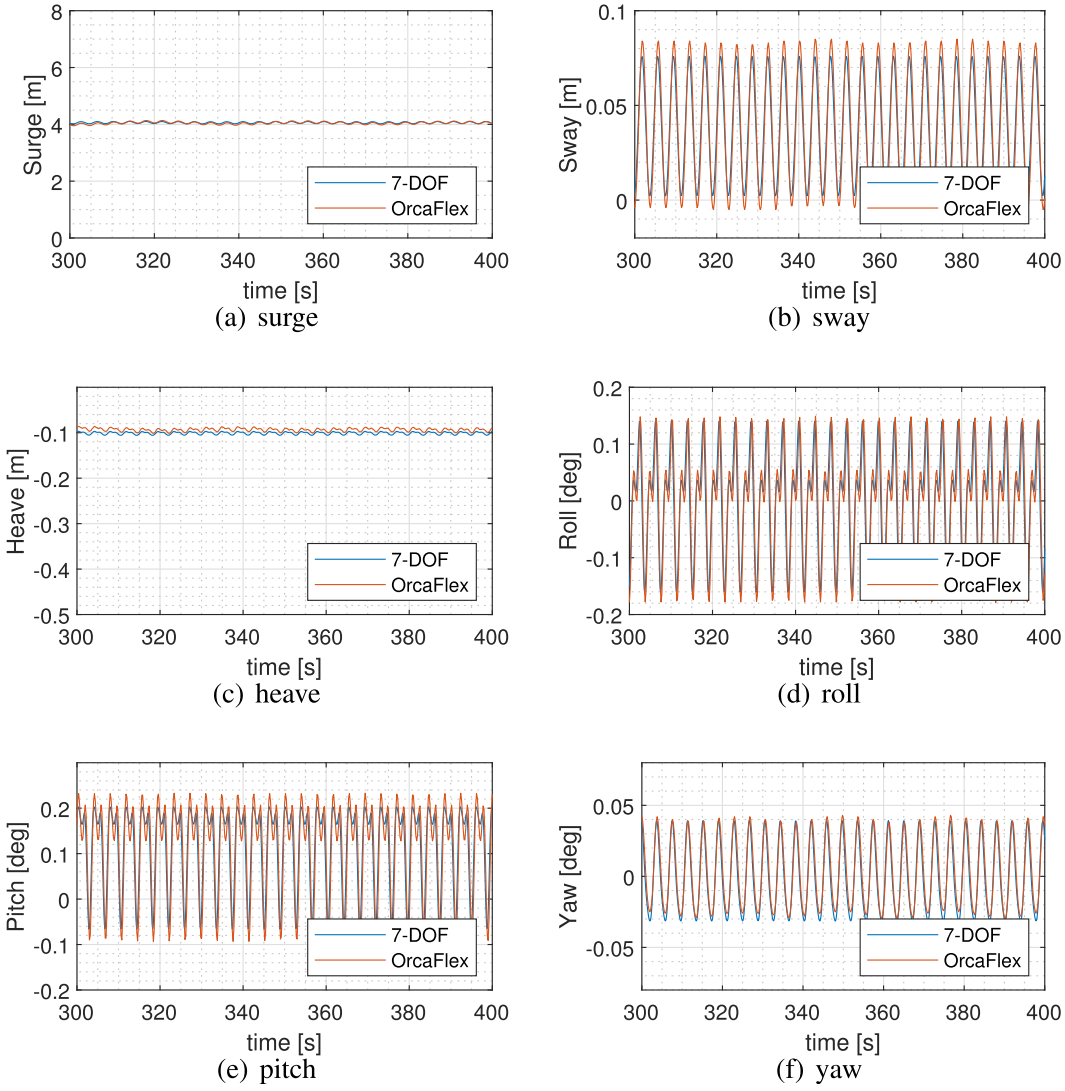

Fig. 6. Comparison of platform motions between OrcaFlex and 7-DOF model under aerodynamic loads.

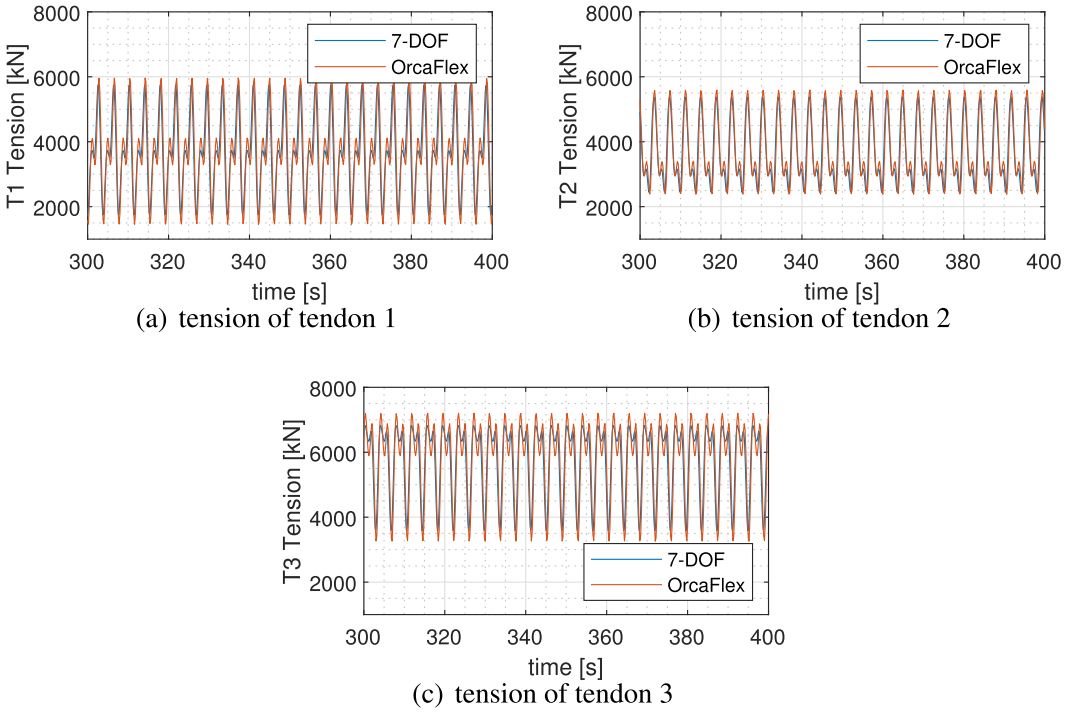

Fig. 7. Comparison of top tensions between OrcaFlex and 7-DOF model under aerodynamic loads.

Both the offset and set-down of 7-DOF(MoorDyn) are slightly greater than those from the other two methods, which demonstrates that the system stiffness calculated from the lumped-mass method is a little softer. 7-DOF(Position) predicts smaller offset (difference within 9%) and greater set-down (difference up to 93%) comparing with the mathematical equation method due to the neglected weight, buoyancy, and wave effects on mooring tendons. In general, the lumped-mass method presents very good agreements with OrcaFlex and mathematical results, thus this method is selected in the subsequent study.

3.3.2. Free decay tests

Free decay tests are performed to validate the 7-DOF model as well as to attain the natural periods of the system. The floating VAWT is under parked condition in still water with no wind considered in the tests. The natural periods and frequencies of the floating VAWT motions estimated using the 7-DOF model are close to those from OrcaFlex as illustrated in Table 4. The greatest natural frequency difference of the 7-DOF model over OrcaFelx is less than 6% in surge and sway motions. The results also show that the natural periods of heave, roll, and pitch falls below the wave excitation zone, which is recommended for a TLP design.

3.3.3. Dynamic responses with turbine aerodynamic loads only

The 7-DOF model is also validated with OrcaFlex based on the dynamic responses of the floating VAWT. Thrust and lateral force shown in Fig. 5 are applied to the turbine pressure center. A total of 240-s ramp time is considered in the simulation.

Platform motions computed from the 7-DOF model generally agree well with OrcaFlex results observed in Fig. 6. Mean values of surge, sway, roll, and pitch of both methods are almost same, but the ranges of these motions of the 7-DOF model are a little less than those of OrcaFlex. The absolute heave of the 7-DOF model is slightly greater than that of OrcaFlex, while mean yaw of the 7-DOF model is less. The differences in platform motions between two methods are caused by the different ways to calculate mooring loads. The lumped-mass method applied in the 7-DOF model neglects wave kinematics, while the sophisticated industrial software OrcaFlex computes mooring loads using the finite element method by considering all the impacts from wave. The comparison of offset vs. set-down also demonstrates that the 7-DOF model underestimates mooring stiffness. Considering the small motions in heave and rotations of TLPs, the 7-DOF model can be applied in prediction of floating VAWT performance and optimization of the system within reasonable fidelity.

Top tensions of the three mooring tendons computed using the two methods are presented in Fig. 7. These tensions from the 7-DOF model are all slightly smaller than those from OrcaFlex. In general, tendon tensions from both methods agree well with each other.

3.3.4. Dynamic responses with both aerodynamic loads and regular wave loads

Dynamic responses of the floating VAWT under both aerodynamic loads and regular wave loads from the 7-DOF model are compared with OrcaFlex. The same aerodynamic loads and ramp time as Section 3.3.3 are applied. A regular wave with a wave height of 5.38 m and period of 11.15 s is also considered.

Comparison of platform motions observed in Fig. 8 shows similar trends as the comparative results under wind load only. Both methods have same mean motions, while the 7-DOF model experiences slightly smaller amplitudes of platform motions than OrcaFlex. Amplitudes of top tensions of all three tendons of the 7-DOF model are a little less than those of OrcaFlex shown in Fig. 9. Although the 7-DOF model slightly underpredicts ranges of platform motions and tendon tensions comparing with OrcaFlex, the overall performance predicted by the 7-DOF model is acceptable.

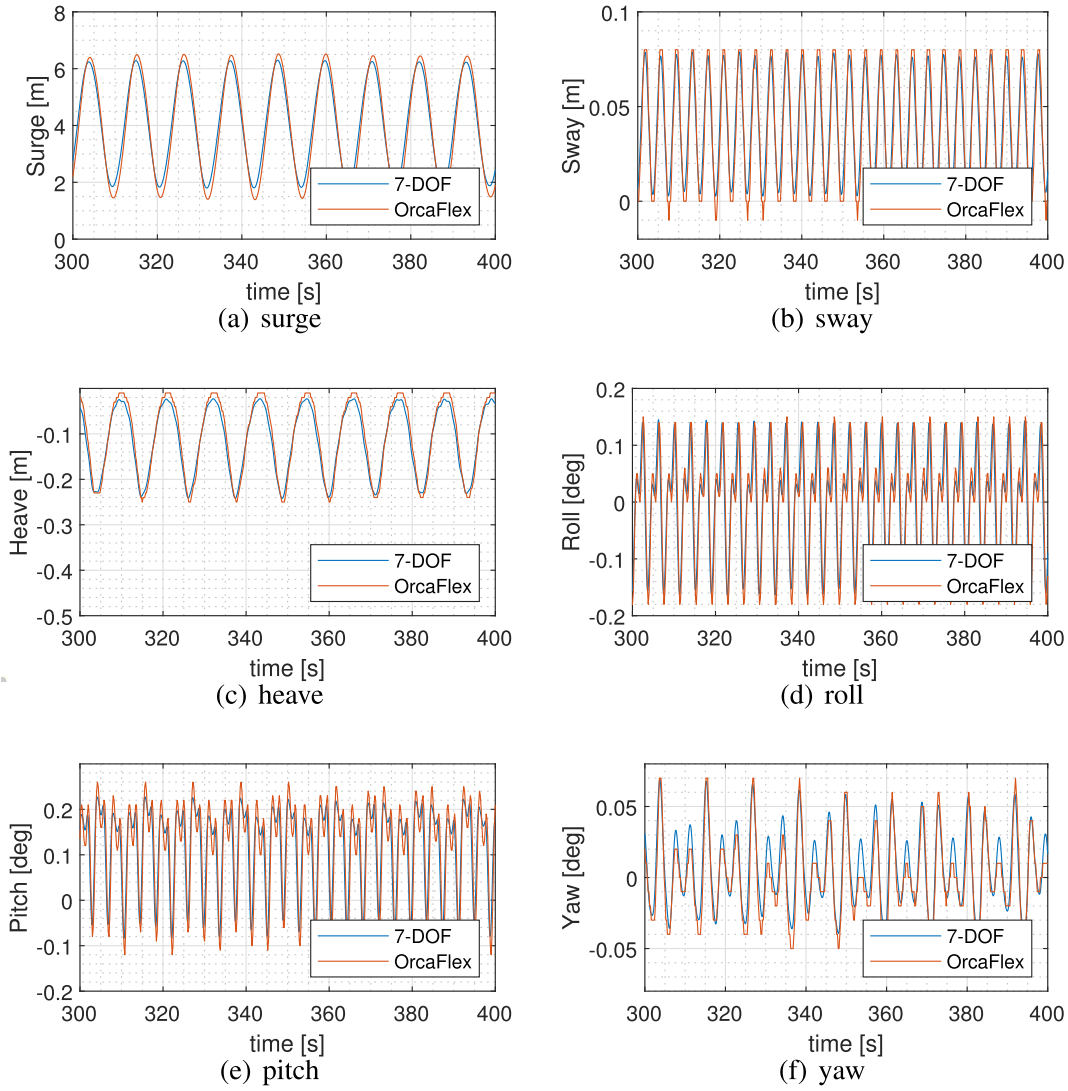

Fig. 8. Comparison of platform motions between OrcaFlex and 7-DOF model under aerodynamic and regular wave loads.

4. Simulation results computed using the 7-DOF model for floating VAWTs

A series of load cases (LCs) are selected to study the performance of the floating VAWTs including the difference between the two- and three-bladed VAWTs. Each simulation in this section is performed for 700 s but the results up to the first 100 s are excluded to minimize the transient effects.

A steady uniform wind field is considered for the operating condition, while wind shear is included in the calculation of the parked drag load for assessment of maximum structural strength. Aerodynamic loads acting on VAWTs increase with the wind speed so the VAWT systems are subject to maximum aerodynamic loads at the cut-out wind speed under operating condition [44]. Thus, performance of the floating VAWTs at this wind speed is evaluated. Fig. 10 shows three aerodynamic load components at the cut-out (25 m/s) wind speed and the parked drag load at the extreme 50-year wind speed of the two- and three-bladed VAWTs, respectively. The overall trend of the comparison of three aerodynamic load components between the two VAWTs at cut-out wind speed is similar to that at the rated wind speed. However, the torque amplitudes of the two VAWTs are close at the cut-out wind speed as shown in Table 5, while the torque amplitude of the two-bladed VAWT is 73% larger than that of the three-bladed VAWT at the rated wind speed. The VAWTs experience constant drag loads at a wind speed greater than the cut-out wind speed since the turbines stop rotating and keep in parked condition. The parked drag load on the two-bladed VAWT is equivalent to a constant 1059 kN load at the aerodynamic pressure center, and the load of the three-bladed VAWT is only 698 kN and 66% of that of the two-bladed VAWT [44]. Therefore it can be estimated that the three-bladed VAWT has the potential to reduce platform motions and tendon tensions over the two-bladed VAWT considering the smaller operational aerodynamic and parked drag loads.

4.1. Impacts from different load components on the floating VAWT

Impacts from different load components on the two-bladed floating VAWT are studied first. This is an important and novel study of the relative contribution of different load components on the floating system performance including operational aerodynamic loads (thrust, lateral, and torque), parked aerodynamic loads, and wave loading. Detailed descriptions of eight LCs are summarized in Table 6 to study these effects. LC1.1 to LC1.7 are for

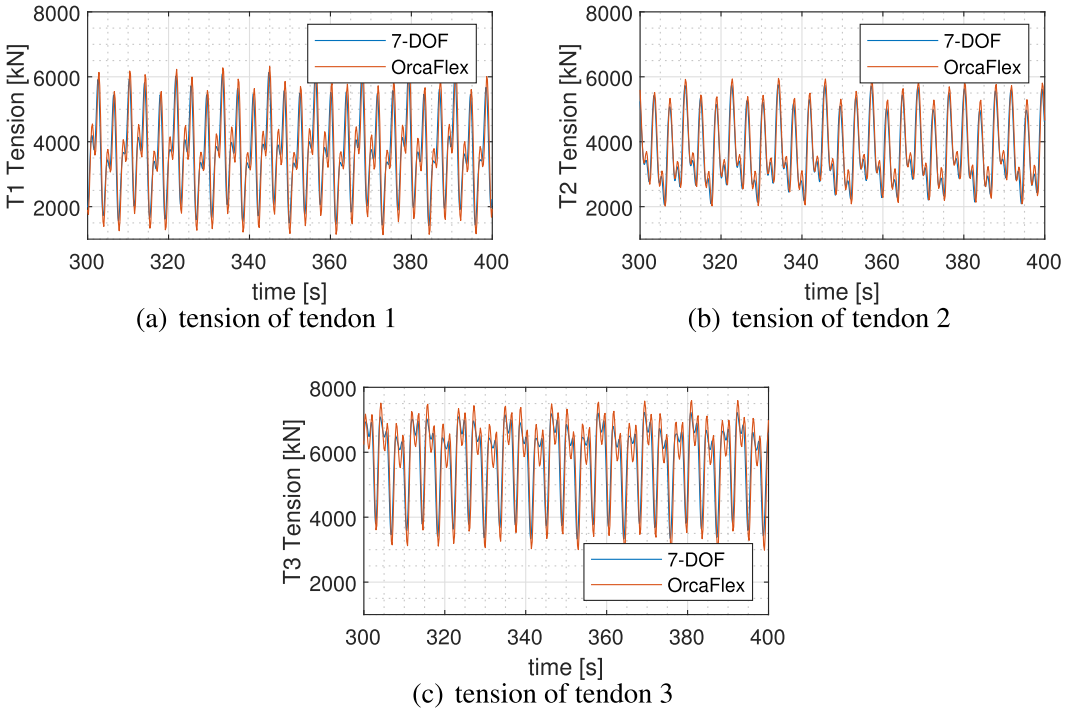

Fig. 9. Comparison of top tensions between OrcaFlex and 7-DOF model under aerodynamic and regular wave loads.

operating condition and LC1.8 is for parked condition. Wind speed in the table represents the wind speed at the aerodynamic pressure center of the turbine. The JONSWAP spectrum with significant wave height and peak wave period is applied to describe irregular waves in this study. Wind and wave in all cases are coincident and along the positive X-axis. Only thrust, only lateral force, only torque, both thrust and lateral force, and all three aerodynamic load components at the cut-out wind speed are considered in LC1.1 to LC1.5, respectively, and no wave excitation load is considered in any of these five LCs. Only the random wave load associated with the cut-out wind speed is applied to the floating VAWT and no wind load is included in LC1.6. Both the three aerodynamic load components and the associated random wave loads are used in LC1.7. A constant parked drag load and associated random wave loads for the extreme 50-year condition are considered in LC1.8. This drag loads on blades and tower are computed with a drag coefficient of 0.82 and a shear coefficient of 0.11 to account for wind shear effect.

Fig. 11 presents the mean displacements and standard deviations of six platform motions of the two-bladed floating VAWT under the eight LCs. The error bars represent positive and negative standard deviation from the mean value. Mean surges in LC1.1, LC1.4, LC1.5, and LC1.7 are observed almost same due to the same thrust. Standard deviations in LC1.1, LC1.4, and LC1.5 are tiny, which demonstrate that the surge motion generated by the periodic thrust varies within a small range. But the standard deviation in LC1.7 is much larger than the other three LCs due to the random wave load. In LC1.6, the irregular wave acting on the platform along surge direction leads to almost zero-mean surge and pitch, but introduces greater variations of motions as predicted by the standard deviations, because the random wave loads acting on the platform have zero mean and large variations. Both mean displacements and standard deviations in surge in LC1.2 and LC1.3 are zero because there is no external load applied along the surge direction. Mean surge and standard deviation in LC1.8 are greater than other cases because of the greater wind and wave loads. Mean sways and standard deviations in LC1.2, LC1.4, LC1.5, and LC1.7 are nonzero due to the lateral force. The coupling between sway and yaw leads to greater mean sway in LC1.5 and LC1.7 than in LC1.2 and LC1.4. Mean surge is much greater than mean sway because the thrust has a positive mean while the lateral force has a close to zero mean. The trend of mean heaves and the associated standard deviations is similar to that of the surge motions. Roll motions are mainly resulted from lateral force, so the platform in LC1.2, LC1.4, LC1.5, and LC1.7 experiences roll motions with non-zero standard deviations and almost zero mean roll due to the zero-mean lateral force. Mean pitch and its standard deviation of each LC is similar to that of surge motion. Yaw motions are mainly resulted from torques, which can be found from LC1.3, LC1.5, and LC1.7.

The maximum top tensions of three tendons under the eight LCs are shown Fig. 12. T1 and T2 in LC1.1 experience same maximum top tensions, while T3 carries greater tensions because thrust is applied along positive X-axis and the system is symmetric about X-axis (Fig. 2). Distribution of the maximum tensions in LC1.2 is also resulted from the tendon positions and direction of lateral force (positive Y-axis). This force contributes more in tendon tensions than the thrust, which is demonstrated by the larger maximum top tension in LC1.2 than that in LC1.1. All tendons experience same maximum tension that is close to the tendon pretension when there is only torque applied to the turbine shown in LC1.3. Maximum tensions of all tendons in LC1.4 and LC1.5 are close, which also demonstrates that torque has little impact on tendons. The trend of maximum tensions in LC1.6 is similar to that in LC1.1 since the wave load is in the same direction as thrust. The maximum tensions of T1 and T3 in LC1.6 are less than those in LC1.5, which indicates that the random wave load leads to smaller impact on tendons than aerodynamic load at the cut-out wind speed. Maximum tensions in LC1.7 are largest among LCs under operating condition due to the combination of wind and wave loads applied to the floating VAWT. The parked drag load and the irregular wave load associated with the extreme wind speed contribute

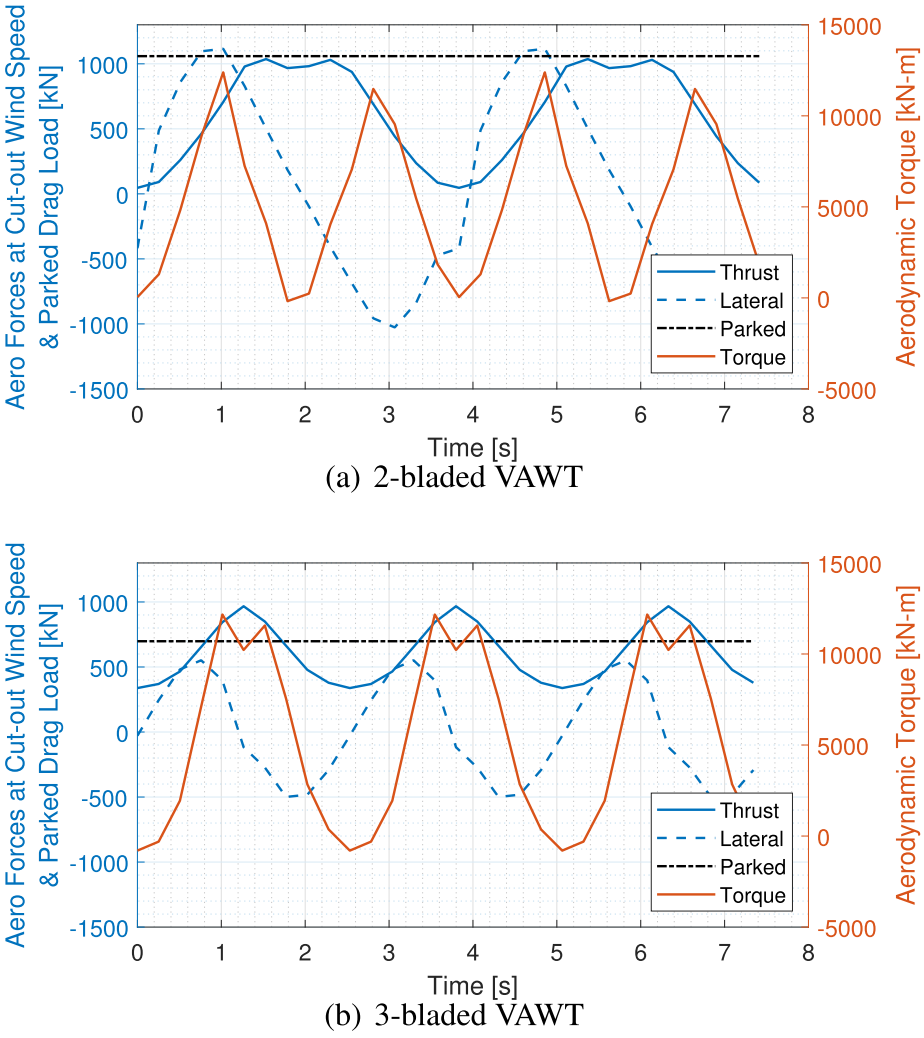

Fig. 10. Three aerodynamic load components at 25 m/s wind speed and parked drag load at extreme 50-year wind speed.

Table 5
Statistics of aerodynamic load components at 25 m/s wind speed.

Aerodynamic Load	Thrust [kN]		Lateral Force [kN]		Torque [kN-m]	
Number of Blades	2	3	2	3	2	3
Maximum	1037	967	1116	552	12388	12167
Minimum	46	338	−1027	−499	−179	−800
Mean	597	601	11	−2	5221	5264

to the largest maximum top tensions among all LCs. Therefore the parking condition associated with extreme environmental condition is critical to strength design of the tendons.

Fig. 13 presents the comparison of minimum tensions of these LCs. Considering both the maximum and minimum tendon tensions, tensions in LC1.3 have tiny variations and are close to pretension, which also verifies that the torque has little impact on tendons. Tension ranges in LC1.1 and LC1.6 are relatively smaller, while tension ranges in LC1.2, LC1.4, LC1.5, and LC1.7 are larger, which demonstrates that the lateral force leads to greater impact on tendons than thrust and wave load at cut-out wind speed. Tendon tensions in LC1.8 experience largest variations due to the parked load and wave load associated with the extreme wind condition. The minimum tensions of tendon 1 in LC1.4 and LC1.5 are greater than but close to zero, and minimum tensions of both

Table 6
Environmental conditions for LC1.1 to LC1.8

Load Case	Wind Speed [m/s]	Wind Load Component	Wave
LC1.1	25.0	Thrust	No wave
LC1.2	25.0	Lateral force	No wave
LC1.3	25.0	Torque	No wave
LC1.4	25.0	Thrust, lateral force	No wave
LC1.5	25.0	Thrust, lateral force, torque	No wave
LC1.6	25.0	N/A	JONSWAP (5.83 m, 11.18s)
LC1.7	25.0	Thrust, lateral force, torque	JONSWAP (5.83 m, 11.18s)
LC1.8	31.1	Parked drag load	JONSWAP (9.80 m, 14.20s)

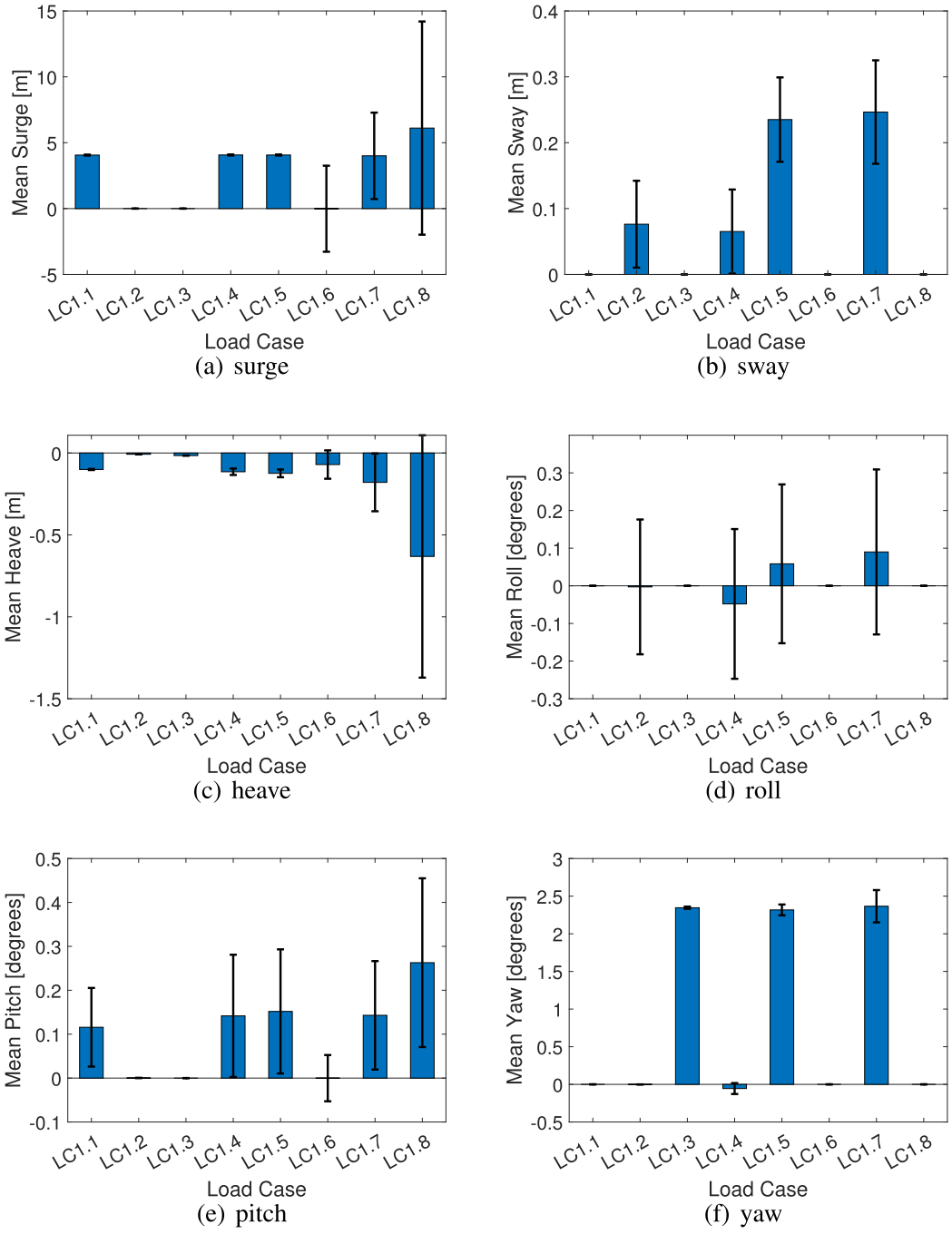

Fig. 11. Mean displacements and standard deviations of the Floating VAWT for LC1.1 to LC1.8.

tendon 1 and 2 in LC1.7 and LC1.8 are close to zero resulted from the greater combined loads acting on the floating system. The tendons used in the current study are initially designed and will be updated for better performance in future work.

In general, most part of the platform offset is contributed by the thrust and the yaw motion is generated by the torque. The lateral force leads to greatest impacts on tendon tensions among operating aerodynamic load components. The random wave load adds variations to the platform motion in the same direction as the wave. The extreme environmental condition dominates the tendon strength design.

4.2. Performance of two-bladed VAWT vs. three-bladed VAWT

The two-bladed floating VAWT has advantages of lower rotor and platform cost and lower center of gravity over the three-bladed turbine illustrated in Tables 1 and 2 However, the larger amplitudes of aerodynamic loads reveal the disadvantage of the two-bladed design. Performance comparison between the two VAWTs is further studied. Three LCs corresponding to the rated, cut-out, and 50-year wind speeds are described in Table 7. Both aerodynamic load and associated irregular wave load are considered in the three LCs. LC2.2 and LC2.3 are same as LC1.7 and LC1.8 in Section 4.1, respectively.

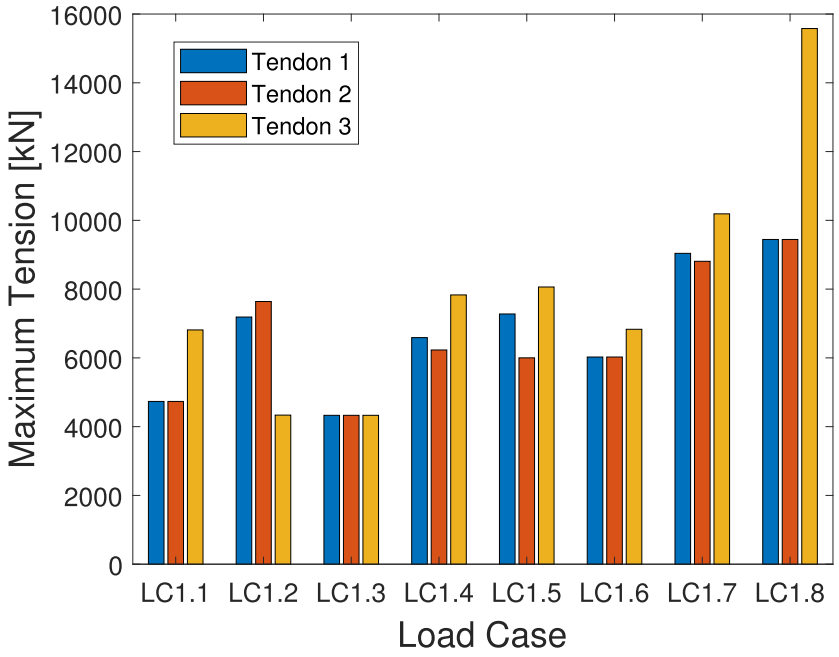

Fig. 12. Maximum top tensions for LC1.1 to LC1.8.

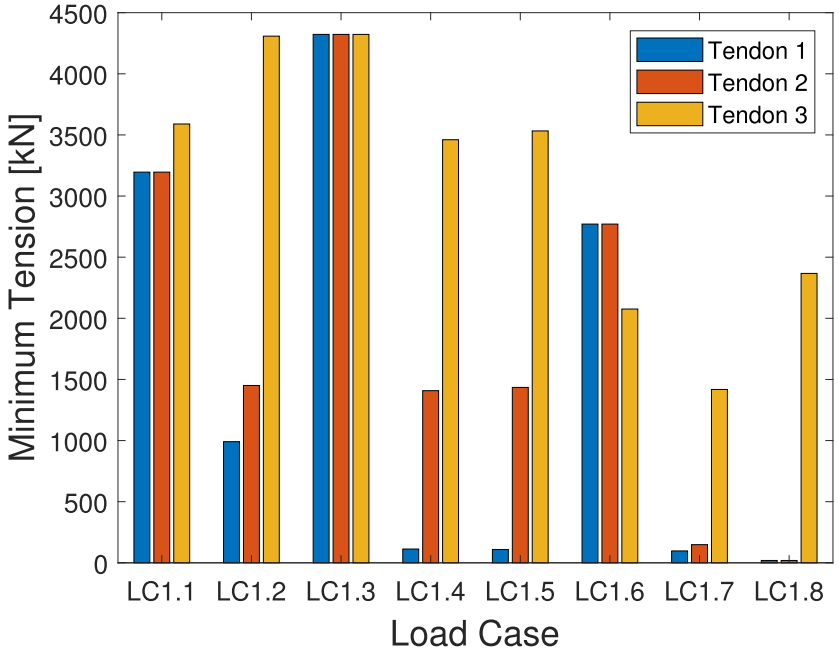

Fig. 13. Minimum tendon tensions for LC1.1 to LC1.8.

Mean motions and standard deviations of all six DOFs of the two-bladed VAWT are larger than those of the three-bladed VAWT for each LC observed from the comparison in Fig. 14, which results from greater aerodynamic loads applied to the two-bladed VAWT as shown in Figs. 3 and 10. Thus the three-bladed floating VAWT has better performance in structural dynamic responses than the two-bladed one. Comparative results between LC2.1 and LC2.2 indicate that greater wind speed generally leads to greater floater motions in all DOFs except yaw under operating conditions. Mean yaw motion of LC2.2 is less than that of LC2.1, but the standard deviation is in opposite trend due to the coupling among the platform motions. The constant parked drag load along the positive X-axis in LC2.3 leads to maximum motions and variations in surge, heave, and pitch comparing with motions in LC2.1 and LC2.2 for both VAWTs.

Table 7
Environmental conditions for LC2.1 to LC2.3

Load Case	Wind Speed [m/s]	Significant Wave Height [m]	Wave peak Period [s]
LC2.1	15.0	3.23	9.14
LC2.2 (LC1.7)	25.0	5.83	11.18
LC2.3 (LC1.8)	31.1	9.80	14.20

Maximum top tensions of the three-bladed VAWT are smaller than those of the two-bladed VAWT illustrated in Fig. 15. T3 has the greatest top tension for each LC due to the wind and wave directions. The percentage differences of the maximum tensions of T3 between the two VAWTs are 7.4%, 10.9%, and 11.6% for LC2.1, LC2.2, and LC2.3, respectively. The better tendon performance provided by the three-bladed VAWT can result in lower tendon costs. Therefore the floating VAWT with three blades has advantages over the turbine with two blades including mitigating platform motions and

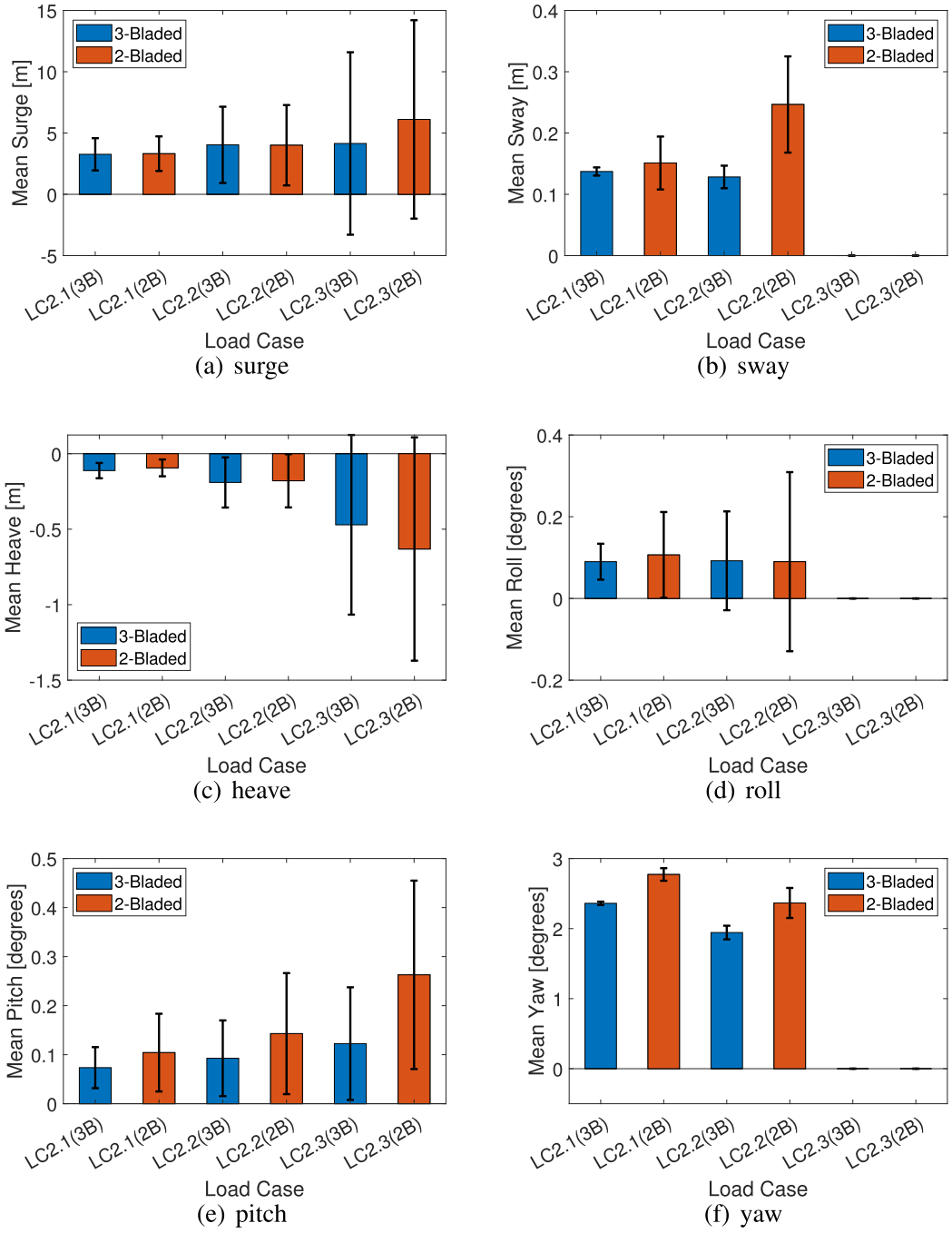

Fig. 14. Mean displacements and standard deviations of the Floating VAWT for LC2.1 to LC2.3.

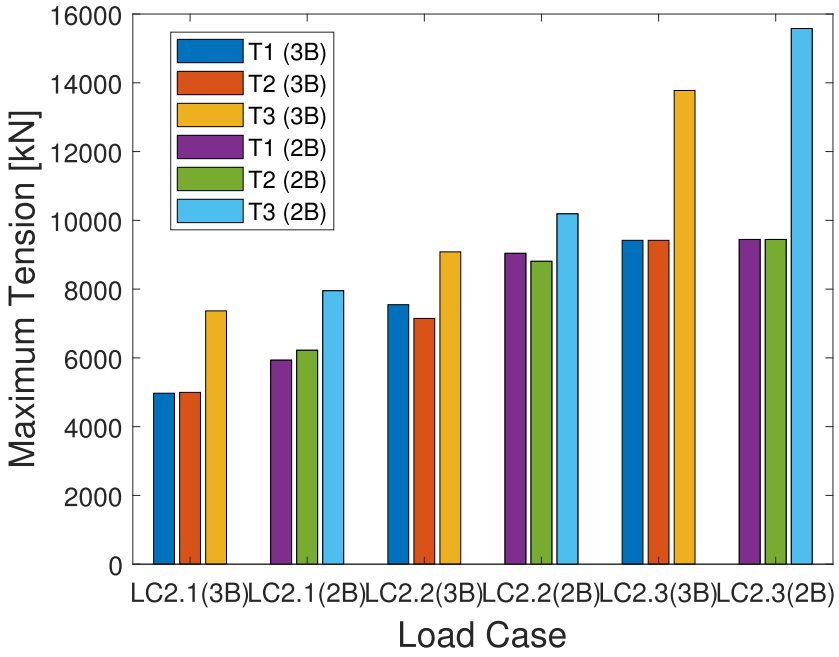

Fig. 15. Maximum top tensions for LC2.1 to LC2.3.

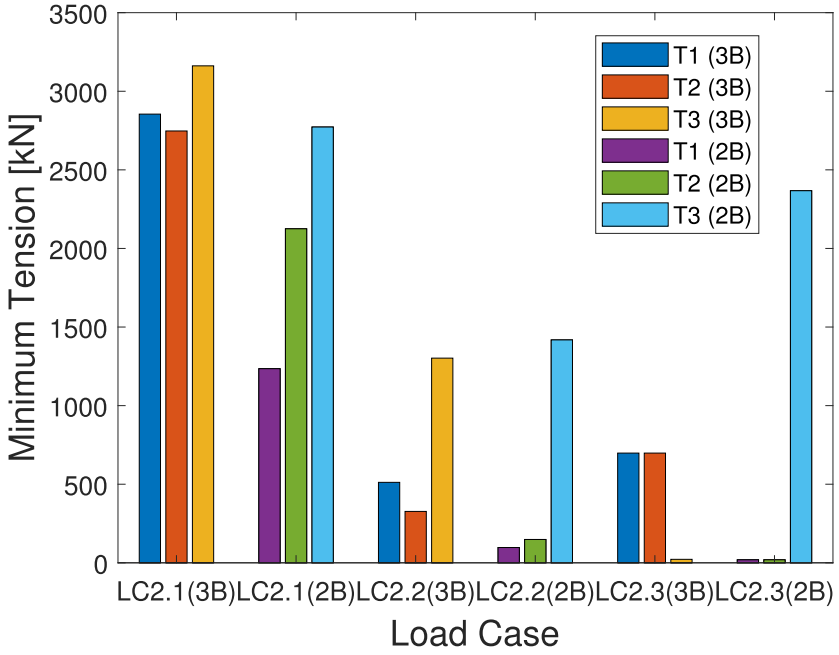

Fig. 16. Minimum top tensions for LC2.1 to LC2.3.

tendon tensions and decreasing tendon costs. Minimum top tensions in all LCs are greater than zero as depicted in Fig. 16. Tension ranges of the three-bladed VAWT are found to be less than those of the two-bladed VAWT for all three LCs calculated from the maximum and minimum tension values, which also demonstrate that the three-bladed VAWT has advantages over the two-bladed one in tendon design.

Comparison of power performance between the two VAWTs is depicted in Fig. 17. Although both VAWTs have same solidity and rated power, the differences in the complex blade wake and blade-strut wake interaction for two-bladed and three-bladed turbines result in different power performance. The three-bladed VAWT generates almost same output power as the two-bladed VAWT at wind speeds below the rated speed, while it generates more power than the two-bladed turbine for greater wind speeds observed from the figure.

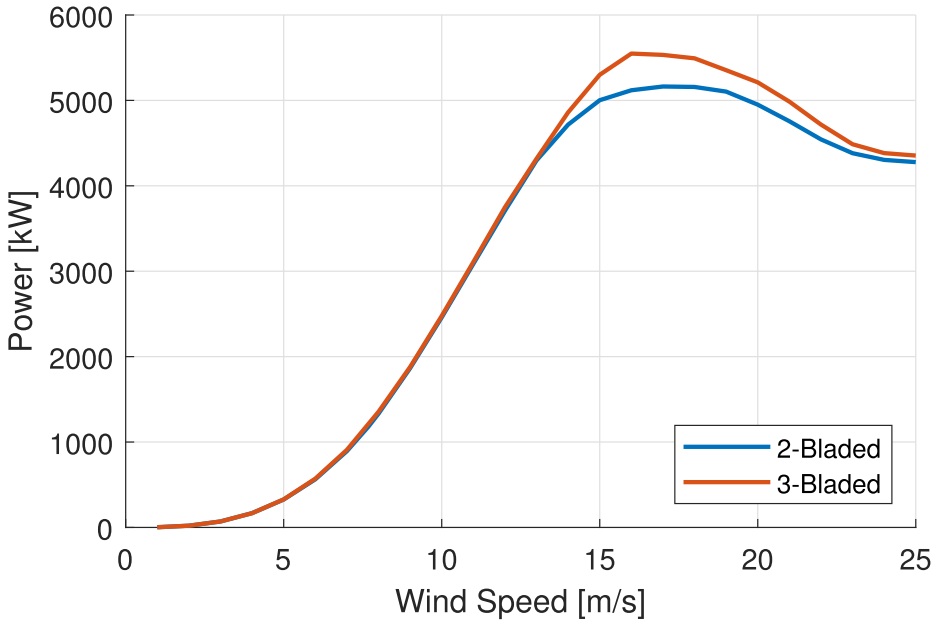

Fig. 17. Power performance of the two- and three-bladed VAWTs at cut-in to cut-out wind speed.

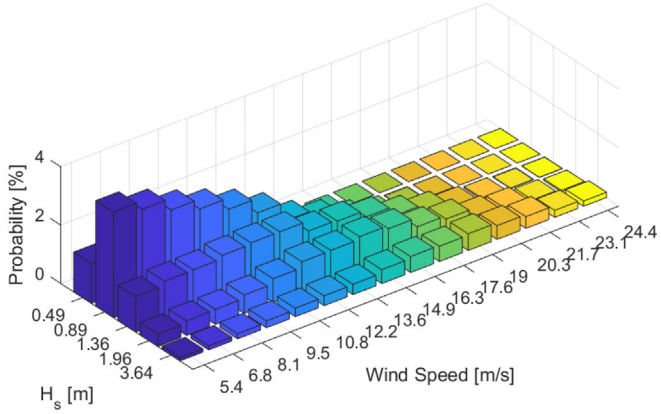

(a) Wind direction = 45 deg

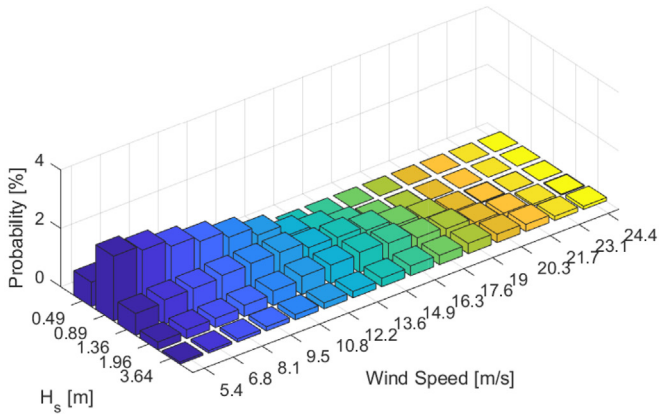

(b) Wind direction = 135 deg

Fig. 18. Wind-wave scatter diagram for tendon fatigue analysis.

4.3. Fatigue analysis of two- and three-bladed floating VAWTs

Aerodynamic loads from the two-bladed turbine introduce strong 2P effects to the system, which is estimated to result in huge fatigue damage on tendons. Similarly aerodynamic loads from the three-bladed turbine cause 3P effects. However, variations of aerodynamic loads of the three-bladed VAWT are much smaller than those of the two-bladed VAWT implying that better fatigue performance of the three-bladed VAWT can be expected. The designed lifetime of both floating VAWTs is 20 years. Fatigue analysis is critical for TLP tendons due to the introduced 2P and 3P effects. Fatigue damage at each tendon top is assessed for both turbines since the maximum tension happens at this location. MLife [50] is applied to compute fatigue damages based on tendon tension time series.

Environmental loading is assumed to be exclusively from uniform winds and associated random waves. Two wind-wave scatter diagrams shown in Fig. 18 depict the sea states used in the fatigue analysis for the wave direction of 150° and the wind directions of 45 and 135°, respectively. The dominant wind direction is 45° based on the probability distributions for the wind speed and wave height as shown in Fig. 18. A total of 150 bins of winds and waves for the fatigue damage evaluation from the diagrams for VAWTs under operating condition are considered. For each fatigue bin, a 700-s simulation is performed with the first 100-s results deleted to mitigate transient effects. Short-term damage rate is computed using MLife for each fatigue bin and each tendon, and then the damage rate is extended to an operation of 20 years based on the wind-wave scatter diagrams.

Considering the impacts from various load components on tendon tensions, influences from different load components on tendon fatigue life are further studied. Six LCs are taken into account in the fatigue analysis. LC3.1 to LC3.6 represent that only thrust, only lateral force, only torque, all three aerodynamic load components, wave load, and both wind and wave loads are considered in the 150 fatigue bins, respectively.

Tendon fatigue damages of both VAWTs are normalized by the maximum fatigue damage of T2 of the two-bladed VAWT. These damages of the two-bladed VAWT are up to 11 times greater than

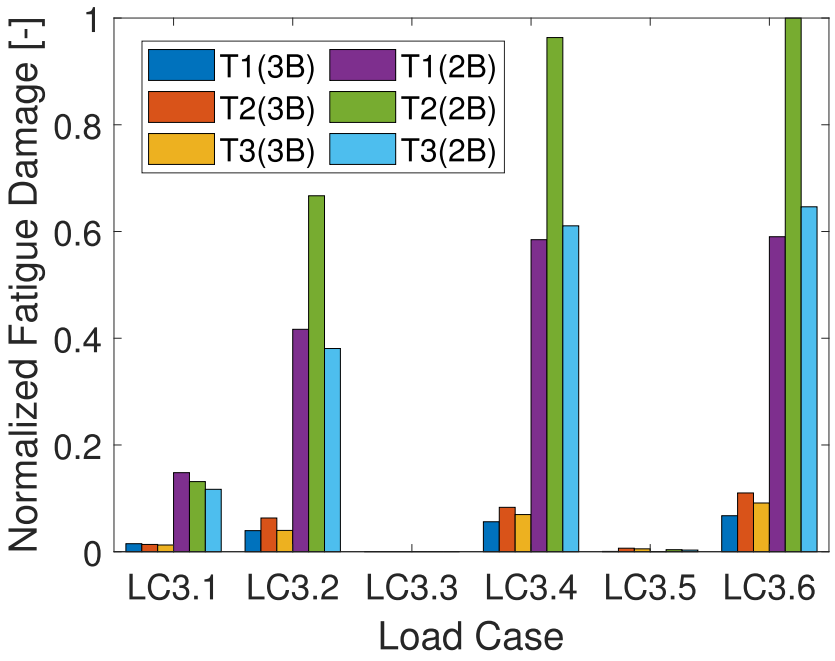

Fig. 19. Normalized fatigue damages of two floating VAWTs for LC3.1 to LC3.6.

Table 8
Environmental conditions for LC4.1 to LC4.4

Load Case	β [−]	Rotor Speed [RPM]	Wind Speed [m/s]	Significant Wave Height [m]	Wave peak Period [s]
LC4.1	N/A	7.8	18.0	4.44	10.12
LC4.2	1.1	Variable	18.0	4.44	10.12
LC4.3	1.0	Variable	18.0	4.44	10.12
LC4.4	0.9	Variable	18.0	4.44	10.12

those of the three-bladed VAWT as illustrated in Fig. 19. Comparison of fatigue damages between two VAWTs in each LC confirms that the three-bladed VAWT has better tendon fatigue performance than the two-bladed VAWT. It is interesting to note that even though the three-bladed VAWT has higher forcing frequency (3P vs 2P) that the significantly smaller cyclic aerodynamic loads for the three-bladed VAWT prevail. Tendon fatigue damages from torque (LC3.3) can hardly be observed from the figure. The wave loads

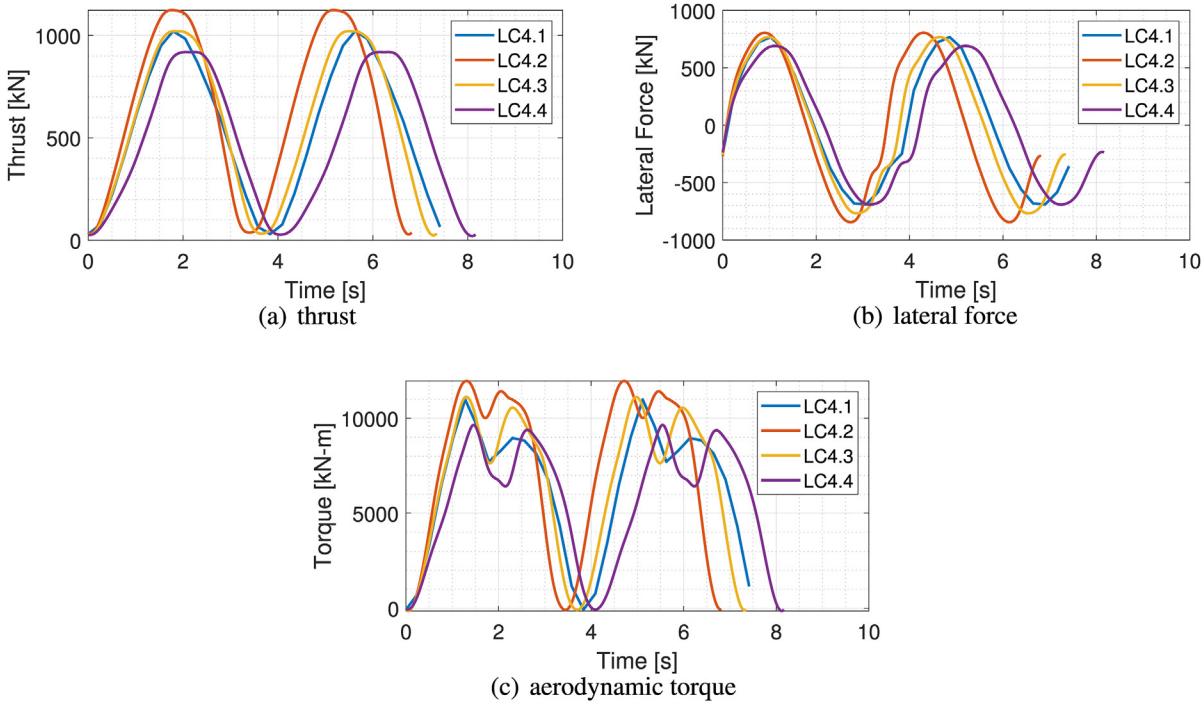

Fig. 20. Comparison of aerodynamic load components of the two-bladed VAWT among LC4.1 to LC4.4.

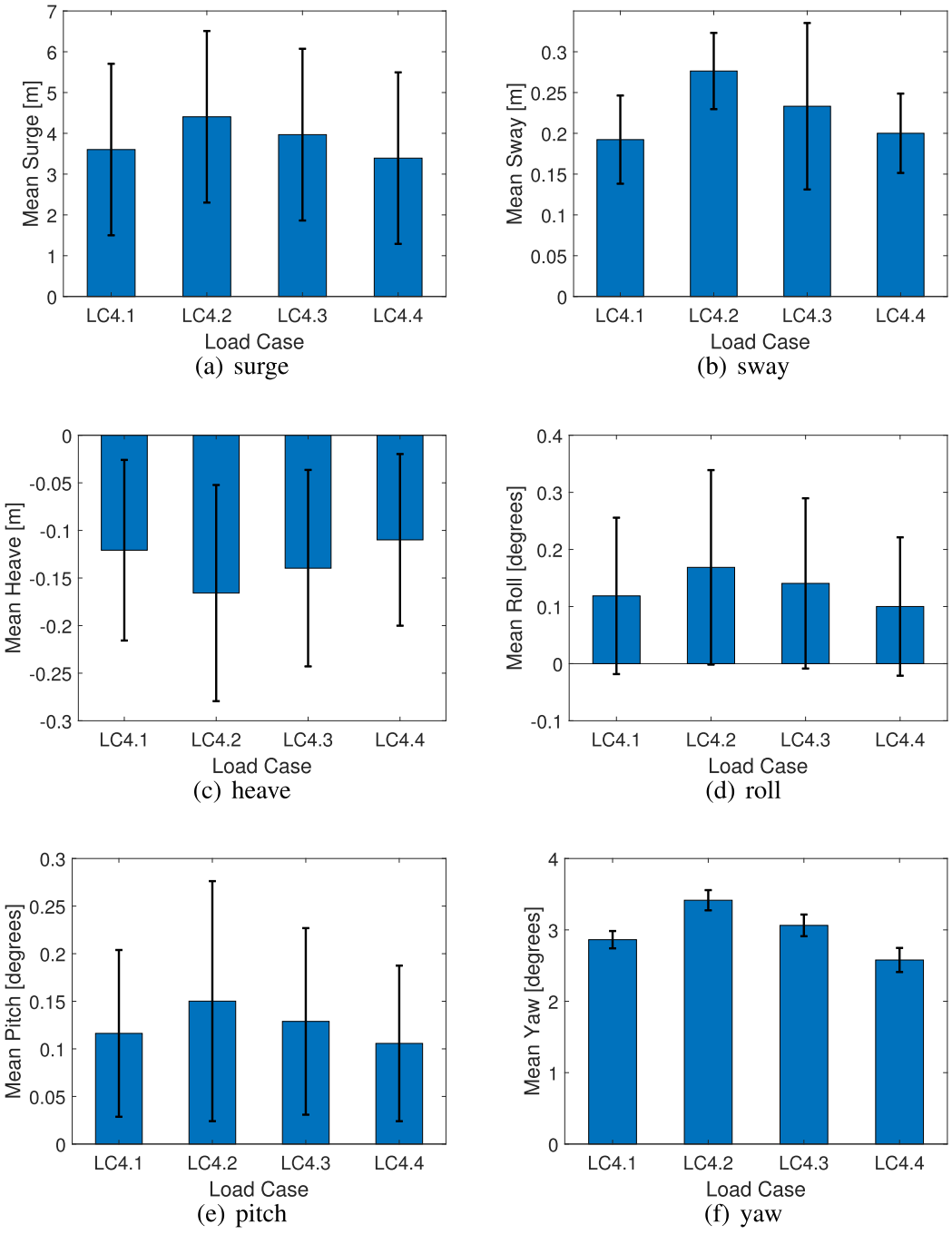

Fig. 21. Mean displacements and standard deviations of the Floating VAWT for LC4.1 to LC4.4.

(LC3.5) lead to little fatigue damage to tendons. The lateral force (LC3.2) is found to dominate tendon fatigue damages when comparing damages in LC3.1, LC3.2, LC3.3, and LC3.5. The thrust (LC3.1) has secondary impact on tendon fatigue damages. Fatigue damage on T2 is significantly greater than that of the other two tendons due to the wind directions.

4.4. Evaluation of intra-cycle RPM control using 7-DOF model for floating VAWTs

One important benefit of the 7-DOF model is its simple way to account for rotor speed control. Intra-cycle RPM control is applied to the two-bladed floating VAWT in order to extract greater power comparing with the turbine without control. Variable rotor speeds are added to the 7th DOF in the 7-DOF model. Four LCs described in Table 8 are selected to evaluate impacts from RPM control on performance of the floating VAWT. No control is applied to the rotor in LC4.1, thus its rotor speed remains constant for the 18 m/s wind speed. This LC is defined as the baseline case. LC4.2 to LC4.4 include intra-cycle RPM control with different non-dimensional constraints (β) on peak values of thrust forces and the rotor speed varying with time in one rotor revolution. The annual energy production (AEP) of LC4.2 and LC4.3 increases 15.3% and 4.6% compared to LC4.1, while AEP of LC4.4 decreases 8.9%. Fig. 20 shows comparison of thrust, lateral force, and aerodynamic torque among these LCs. LC4.2 with a constraint greater than 1.0 has largest aerodynamic loads, LC4.4

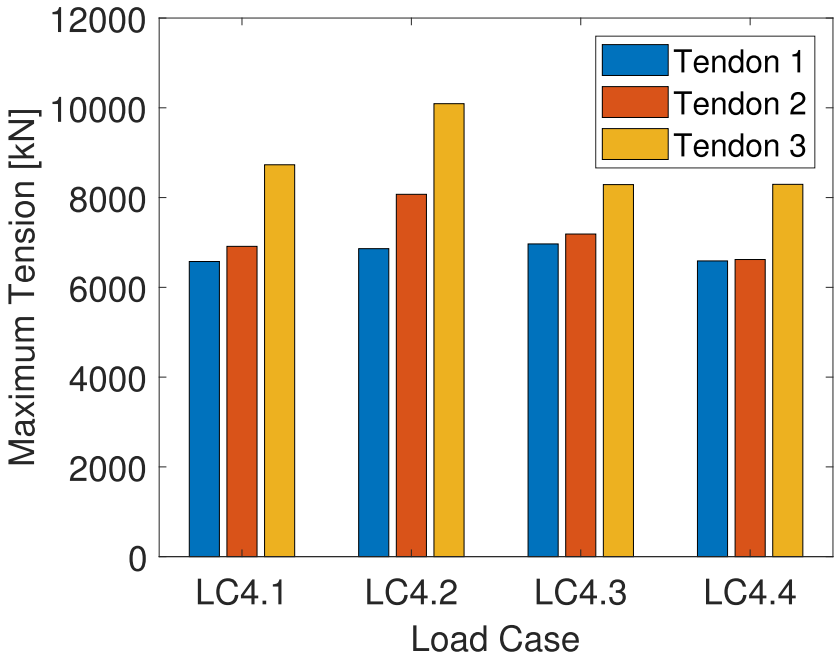

Fig. 22. Maximum top tensions of the Floating VAWT for LC4.1 to LC4.4.

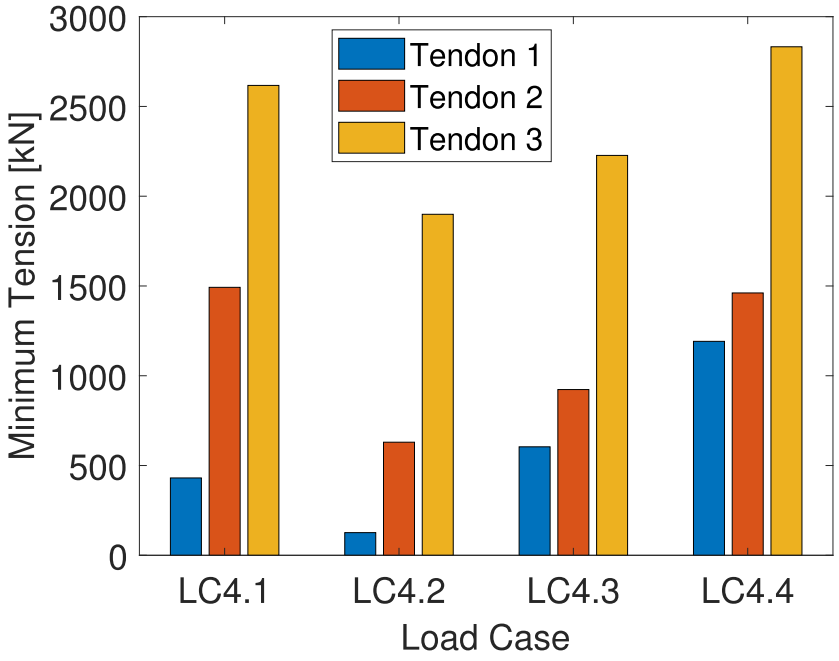

Fig. 23. Minimum top tensions of the Floating VAWT for LC4.1 to LC4.4.

has smallest loads due to its constraint less than 1.0, and LC4.3 with a constraint of 1.0 has similar wind loads as LC4.1.

Greater constraint value in the RPM control results in not only more power but also larger platform motions, which can be found from the mean platform motions in six DOFs shown in Fig. 21. Mean surges of LC4.2 to LC4.4 are 22.3%, 10.1%, and −5.8% different from that of LC4.1. Other motions have even greater percentage difference between LCs with and without control. Figs. 22 and 23 present maximum and minimum top tension comparison of the three tendons among the four LCs, respectively. Trends of these tensions are similar to those of mean platform motions, e.g., LC4.2 and LC4.4 predict the greatest and smallest maximum top tensions as well as tension ranges among the four LCs, respectively.

The trade-off between the AEP and the structural dynamic performance of the floating VAWT is found through the above comparative results. The AEP of LC4.2 increases a lot comparing

with the baseline case LC4.1 through the RPM control, but LC4.2 results in greater platform motions and tendon tensions, which makes it not a suitable control design. Structural dynamic performance of LC4.3 is a little worse than that of the baseline case, but a greater AEP is achieved. LC4.4 has the smallest platform motions and least AEP. This work demonstrates the value of the 7-DOF model to study AEP versus loads trade-offs; however, further study is needed to find a balance between the generated power and the dynamic performance of the floating VAWT.

5. Conclusions

A new semi-coupled aero-servo-hydro 7-DOF model has been developed to predict dynamic responses of a TLP type floating VAWT platform. The 7-DOF system is established with consideration of the six DOFs of rigid motions and 7th DOF of the rotor rotation. Aerodynamic loads input to this model are computed using the free wake vortex method, hydrodynamic loads are calculated using diffraction method, the viscous drag load acting on the platform is considered with the Morison equation, and mooring loads are calculated with the lumped-mass method. The 7th DOF is coupled with the other six DOFs through generator torque. A simple intra-cycle RPM control is applied to the 7th DOF in order to enhance output power. Utilization of this model is not restricted to TLP-type floaters. It can also be adjusted to evaluate performance of floating VAWTs with other types of supporting platforms if large rotational motions exist. Low complexity and computational cost enable the 7-DOF model to be utilized in the design process of floating VAWTs efficiently.

This model is validated with OrcaFlex through various case-by-case tests. Validations are first made through the static offset vs. set-down and free decay tests. Additional dynamic results from the aerodynamic and regular wave loads are compared. The comparative results demonstrate that the 7-DOF model predicts offset vs. set-down very well, natural frequencies of the floating VAWT within 6% difference, and platform motions and tendon tensions generally well. This model slightly overpredicts surge and heave motions due to neglecting wave kinematics on mooring tendons. Considering the simpleness and small computational cost, the 7-DOF model can be used to design and optimize floating VAWTs with reasonable fidelity.

Structural dynamic performance of two newly designed floating VAWTs is predicted using this 7-DOF model. At first, comparative results from various load components on the two-bladed floating VAWT reveal that platform offset is mainly generated by the thrust acting on the rotor with a positive mean along the wind direction. The lateral force introduces a much smaller mean motion comparing with thrust due to its close to zero-mean value; however, it has greatest impacts on tendon tensions than other load components. The torque leads to platform yaw motion and introduces little effect on tendon tensions. Wave loads add variations to the platform motions but barely influence the mean motions. The parked drag load with its associated random wave load under extreme environmental condition leads to greatest platform motions as well as maximum tendon tensions, which is an important factor to strength design of tendons. Moreover, comparison of the platform motions, maximum tendon tensions, generated power, and fatigue damages at tendon tops between the two- and three-bladed VAWTs demonstrates that the three-bladed VAWT has great advantages of better structural dynamic and power performance and much longer fatigue life over the two-bladed VAWT. Therefore a three-bladed rotor is preferred for a floating VAWT design. Finally, study of dynamic responses of the floating VAWT under intra-cycle RPM control proves the ability of the 7-DOF model to be used for rotor control.

CRediT authorship contribution statement

Ju Gao: Methodology, Software, Validation, Formal analysis, Investigation, Writing – original draft, Visualization. **D. Todd Griffith:** Conceptualization, Methodology, Resources, Writing – review & editing, Supervision, Project administration, Funding acquisition. **Mohammad Sadman Sakib:** Resources, Writing – review & editing. **Sung Youn Boo:** Validation, Resources, Writing – review & editing.

Declaration of competing interest

The authors declare that they have no known competing financial interests or personal relationships that could have appeared to influence the work reported in this paper.

Acknowledgment

The research presented herein was funded by the US Department of Energy Advanced Research Projects Agency-Energy (ARPA-E) under the ATLANTIS program with project title “A Low-cost Floating Offshore Vertical Axis Wind System” with Award No. DE-AR0001179. Any opinions, findings, and conclusions or recommendations expressed in this material are those of the authors and do not necessarily reflect the views of ARPA-E. The authors are grateful for the support of the ARPA-E program and staff, and the project team.

References

[1] M. Borg, M. Collu, F.P. Brennan, Offshore floating vertical axis wind turbines: advantages, disadvantages, and dynamics modelling state of the art, in: Marine and Offshore Renewable Energy, 2012, pp. 26–27.
[2] D.T. Griffith, M. Barone, J. Paquette, B. Owens, D. Bull, C. Simao-Ferriera, A. Goupee, M. Fowler, Design Studies for Deep-Water Floating Offshore Vertical axis Wind Turbines, Tech. Rep. SAND2018-7002, Sandia National Laboratories, 2018.
[3] D.T. Griffith, J. Paquette, M. Barone, A.J. Goupee, M.J. Fowler, D. Bull, B. Owens, A study of rotor and platform design trade-offs for large-scale floating vertical axis wind turbines, in: Journal of Physics: Conference Series, vol. 753, 2016, p. 102003.
[4] J.M. Jonkman, M.L. Buhl Jr., FAST User's Guide, Tech. Rep. NREL/EL-500-38230, National Renewable Energy Laboratory, 2005.
[5] OpenFAST, https://www.nrel.gov/wind/nwtc/openfast.html ((accessed Jun. 14, 2021)).
[6] Y.H. Bae, M.H. Kim, Rotor-floater-tether coupled dynamics including second-order sum-frequency wave loads for a mono-column-TLP-type FOWT (Floating Offshore Wind Turbine), Ocean Eng. 61 (2013) 109–122.
[7] Y. Yang, M. Bashir, C. Michailides, C. Li, J. Wang, Development and application of an aero-hydro-servo-elastic coupling framework for analysis of floating offshore wind turbines, Renew. Energy 161 (2020) 606–625.
[8] ANSYS, AQWA Reference Manual Release, 14.5, ANSYS, Inc., 2012.
[9] DNV-GL, Wind turbine design software-Bladed, https://www.dnvgl.com/services/wind-turbine-design-software-bladed-3775 ((accessed Apr. 7, 2021))..
[10] A. Beardsell, A. Alexandre, B. Child, R. Harries, D. McCowen, Beyond OC5-further advances in floating wind turbine modelling using Bladed, J. Phys. Conf. 1102 (1) (2018).
[11] WAMIT, https://www.wamit.com/manual6.htm ((accessed Apr. 7, 2021)).
[12] L. Wang, B. Sweetman, Simulation of large-amplitude motion of floating wind turbines using conservation of momentum, Ocean Eng. 42 (2012) 155–164.
[13] J. Gao, B. Sweetman, Design optimization of hull size for spar-based floating offshore wind turbines, J. Ocean Eng. Mar. Energy 4 (2018) 217–229.
[14] J. Chen, Z. Hu, G. Liu, D. Wan, Coupled aero-hydro-servo-elastic methods for floating wind turbines, Renew. Energy 130 (2019) 139–153.
[15] M.I. Kvittem, E.E. Bachynski, T. Moan, Effects of hydrodynamic modelling in fully coupled simulations of a semi-submersible wind turbine, in: DeepWind, 2012.
[16] HAWC2, https://www.hawc2.dk/((accessed Apr. 7, 2021)).
[17] C.L. Cunff, J.-M. Heurtier, L. Piriou, C. Berhault, T. Perdrizet, D. Teixeira, G. Ferrer, J.-C. Gilloteaux, Fully coupled floating wind turbine simulator based on nonlinear finite element method-Part I: Methodology, in: ASME 2013 32nd International Conference on Ocean, Offshore and Arctic Engineering, 2013.
[18] T. Perdrizet, Jean-Christophe, D. Teixeira Gilloteaux, G. Ferrer, L. Piriou, D. Cadiou, J.-M. Heurtier, C.L. Cunff, Fully coupled floating wind turbine

simulator based on nonlinear finite element method-Part II: validation results, in: ASME 2013 32nd International Conference on Ocean, Offshore and Arctic Engineering, 2013.
[19] Y. Chen, A.S. Mendoza, D.T. Griffith, Experimental and numerial study of high-order complex curvature mode shape and mode coupling on a three-bladed wind turbine assembly, Mech. Syst. Signal Process. 160 (2021) submitted for publication.
[20] J.C. Murray, M. Barone, The development of CACTUS, a wind and marine turbine performance simulation code, in: 49th AIAA Aerospace Sciences Meeting Including the New Horizons Forum and Aerospace Exposition, 2011.
[21] T.J. Larsen, H.A. Madsen, On the way to reliable aeroelastic load simulation on VAWT's, in: EWEA 2013 European Wind Energy Association (EWEA), 2013.
[22] D. Marten, J. Wendler, G. Pechlivanoglou, C. Nayeri, C. Paschereit, QBlade: an open source tool for design and simulation of horizontal and vertical axis wind turbines, Int. J. Emerg. Technol. Adv. Eng. 3 (2013) 264–269.
[23] D. Marten, G. Pechlivanoglou, C. Nayeri, C.O. Paschereit, Nonlinear lifting line theory applied to vertical axis wind turbines: development of a practical design tool, in: International Symposium on Transport Phenomena and Dynamics of Rotating Machinery, 2016.
[24] B.C. Owens, J.E. Hurtado, J.A. Paquette, D.T. Griffith, M. Barone, Aeroelastic modeling of large offshore vertical-axis wind turbines: development of the offshore wind energy simulation toolkit, in: 54th AIAA/ASME/ASCE/AHS/ASC Structures, Structural Dynamics, and Materials Conference, 2013.
[25] M. Collu, M. Borg, A. Shires, F.P. Brennan, FloVAWT: progress on the development of a coupled model of dynamics for floating offshore vertical axis wind turbines, in: The ASME 2013 32nd International Conference on Ocean, Offshore and Arctic Engineering, 2013.
[26] M. Borg, M. Collu, A comparison on the dynamics of a floating vertical axis wind turbine on three different floating support structures, Energy Procedia 53 (2014) 268–279.
[27] M. Collu, M. Borg, A. Shires, F.N. Rizzo, E. Lupi, FloVAWT: further progresses on the development of a coupled model of dynamics for floating offshore VAWTs, in: The ASME 2014 33rd International Conference on Ocean, Offshore and Arctic Engineering, 2014.
[28] K. Wang, T. Moan, M.O.L. Hansen, A method for modeling of floating vertical axis wind turbine, in: ASME 2013 32nd International Conference on Ocean, Offshore and Arctic Engineering, 2013.
[29] Z. Cheng, K. Wang, Z. Gao, T. Moan, Dynamic response analysis of three floating wind turbine concepts with a two-bladed Darrieus rotor, J. Ocean Wind Energy 2 (4) (2015) 213–222.
[30] D. Pitance, S. Horb, J. Kluczewska-Bordier, A. Immas, F. Silvert, Experimental validation of PHARWEN code using data from vertical-axis wind turbines, in: EWEA, 2016.
[31] A. Thibierge, Validation of a Vortex Panel Method for Aerodynamics and Aero-Elasticity of Wind Turbine, Master's Thesis, KTH Royal Institute of Technology, Stockholm, Sweden, 2018.
[32] Z. Cheng, H.A. Madsen, Z. Gao, T. Moan, A fully coupled method for numerical modeling and dynamic analysis of floating vertical axis wind turbines, Renew. Energy 107 (2017) 604–619.
[33] V. Leroy, J.-C. Gilloteaux, M. Philippe, A. Babarit, P. Ferrant, Servo-hydro and unsteady aerodynamic simulation of floating vertical axis wind turbines, in: 23e Congrès Français de Mécanique, 2017.
[34] A. Combourieu, M. Philippe, F. Rongère, A. Babarit, InWave, A new flexible design tool dedicated to Wave Energy Converters, in: The ASME 2014 33rd International Conference on Ocean, Offshore and Arctic Engineering, 2014.
[35] OrcaFlex, https://www.orcina.com/orcaflex/((accessed Apr. 7, 2021)).
[36] L. Vita, U.S. Paulsen, T.F. Pedersen, H.A. Madsen, F. Rasmussen, A novel floating offshore wind turbine concept, in: EWEC, 2009.
[37] U.S. Paulsen, L. Vita, H.A. Madsen, J. Hattel, E. Ritchie, K.M. Leban, P.A. Berthelsen, S. Carstensen, 1st Deepwind 5 MW baseline design, in: DeepWind, 2012.
[38] U.S. Paulsen, H.A. Madsen, J.H. Hattel, I. Baran, P.H. Nielsen, Design optimization of a 5 MW floating offshore vertical-axis wind turbine, in: DeepWind, 2013.
[39] H. Akimoto, K. Tanaka, K. Uzawa, Floating axis wind turbines for offshore power generation-a conceptual study, Environ. Res. Lett. 6 (2011).
[40] H.J. Sutherland, D.E. Berg, T.D. Ashwill, A Retrospective of VAWT Technology, Tech. Rep. SAND2012-0304, Sandia National Laboratories, 2012.
[41] F. Savenije, S4VAWT final report, Tech. Rep. TNO (2018). R11359, TNO (2018).
[42] Capytaine: a Python-based distribution of Nemoh, https://ancell.in/capytaine/latest/((accessed Apr. 7, 2021)).
[43] M. Hall, A. Goupee, Validation of a lumped-mass mooring line model with DeepCwind semisubmersible mode test data, Ocean Eng. 104 (2015) 590–603.
[44] M.S. Sakib, D.T. Griffith, Parked and operating loads analysis in the aerodynamic design of multi-megawatt-scale floating vertical axis wind turbines, Wind Energ. Sci. Discuss (2021), https://doi.org/10.5194/wes-2021-60 submitted for publication.
[45] S.Y. Boo, S.A. Shelley, D. Kim, A TLP floating foundation design with novel tendon mooring technology for Hawaii offshore wind, in: 29th ISOPE Conference, 2019.
[46] S.Y. Boo, S.A. Shelley, D. Kim, Concept design of floating wind platforms of Y-wind and T-wind for south east offshore of Korea, in: Korea Wind Energy Association, Fall Conference, 2018.
[47] F. Ahsan, D.T. Griffith, J. Gao, Modal Dynamics and Flutter Analysis of Floating Offshore Vertical axis Wind Turbine Rotors, Renewable Energy, 2021 submitted for publication.
[48] X. hui Zeng, X. peng Shen, Y. xiang Wu, Governing equations and numerical solutions of tension leg platform with finite amplitude motion, Appl. Math. Mech. 28 (1) (2007) 37–49.
[49] Z. Demirbilek, Design formulae for offset, set down and tether loads of a tension leg platform (TLP), Ocean Eng. 17 (5) (1990) 517–523.
[50] MLife, https://www.nrel.gov/wind/nwtc/mlife.html ((accessed Jun. 14, 2021)).